Reviews

Nanozeolites: Synthesis, Crystallization Mechanism, and Applications

Lubomira Tosheva and Valentin P. Valtchev*

Laboratoire de Matériaux à Porosité Contrôlée, UMR-7016 CNRS, ENSCMu, Université de Haute Alsace, 3, rue Alfred Werner, 68093 Mulhouse Cedex, France

Received December 1, 2004. Revised Manuscript Received February 4, 2005

This review focuses on the synthesis, crystallization mechanism, and application of colloidal zeolites. The synthesis formulations and features of different zeolite-type structures prepared in nanosized form are summarized. Special attention is paid to zeolites prepared as stable colloidal suspensions. Next, new insights into zeolite crystallization mechanism gained by using colloidal zeolites as model systems are discussed. Further, the methods for deposition of zeolite nanocrystals from suspensions onto supports of different shapes and compositions used for the fabrication of zeolite films and membranes are reviewed. The use of colloidal zeolites for the fabrication of hierarchical macrostructures is also described. Other uses of nanozeolites for the preparation of functionalized materials, for the synthesis of mesoporous silicas of improved hydrothermal stability, and as seeds for zeolite syntheses are illustrated. The emerging applications of nanozeolites in sensing, optoelectronics, and medicine constitute another topic in this review. Finally, some future trends in the area are envisaged.

Introduction

In the past 3 years several excellent review articles dedicated to different aspects of zeolite synthesis, recent developments, and applications appeared.[1−4] None of them was, however, entirely dedicated to the area of zeolite nanocrystals. Considering the expanding interest in the subject, the growing number of zeolites prepared in a nanosized form and the emerging applications of zeolite nanocrystals or zeolite nanocrystal-built materials, such a review should be of great interest not only for the zeolite community but also for collaborating scientists from interdisciplinary fields.

The nanosized zeolites considered in this review have a size of less than 1000 nm. Special attention is paid to colloidal suspensions of zeolites with narrow particle size distributions and sizes of less than 200 nm. These suspensions are colloidally stable and the dispersed zeolites do not settle down for long periods of time, e.g., more than 6 months. The suspensions also show the Tyndall light-scattering effect. An example of such a suspension is the suspension of silicalite-1 (MFI-type structure) with an average size of 60 nm and whose narrow particle size distribution as determined by dynamic light scattering is shown in Figure 1. Besides the benefits of colloidal zeolites over conventional zeolites related to their small crystal size, the major interest in colloidal zeolite suspensions is due to their use for preparation of zeolite films and membranes as well as composites and hierarchical structures. The colloidal size of the crystals employed in such preparations brings unique properties to the structures prepared and expand the area of zeolite applications toward, e.g., optoelectronics, chemical sensing, and medicine. From a fundamental point of view, the systems are convenient for studying the zeolite crystallization mechanism by methods not applicable in conventional zeolite syntheses. For instance, the in situ dynamic light scattering measurements allow tracking down of the evolution of the particle size as a function of the synthesis time.

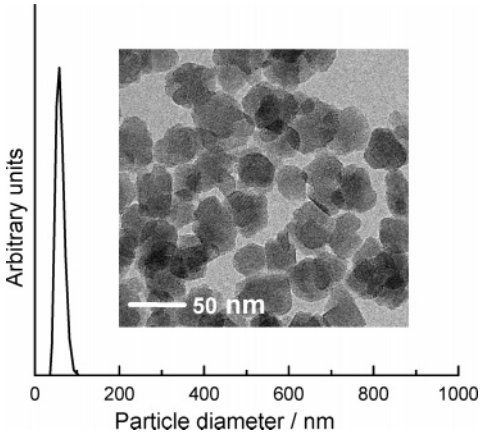

Figure 1. Particle size distribution by volume of an aqueous suspension of silicalite-1 determined by dynamic light scattering. The inset shows the corresponding TEM image.

The reduction of particle size from the micrometer to the nanometer scale leads to substantial changes in the properties of the materials, which have an impact on the performance

* To whom correspondence should be addressed. E-mail: V.Valtchev@uha.fr.

10.1021/cm047908z CCC: $30.25 © 2005 American Chemical Society
Published on Web 04/09/2005

of zeolites in traditional application areas such as catalysis and separation. Thus, the ratio of external to internal number of atoms increases rapidly as the particle size decreases and zeolite nanoparticles have large external surface areas and high surface activity. The external surface acidity is of importance when the zeolite is intended to be used as a catalyst in reactions involving bulky molecules. In addition, smaller zeolite crystals have reduced diffusion path lengths relative to conventional micrometer-sized zeolites.

The present review is divided into three parts. The first part summarizes the methods reported for the synthesis of zeolite nanocrystals of different structural types. In the second part, the new insights into the crystallization mechanism of zeolites gained by employing colloidal zeolites as model systems are reviewed. The final part is devoted to applications of nanozeolites for the synthesis of composite and hierarchical materials and other zeolite materials, and nonconventional applications of zeolite nanocrystals or nanocrystal-based materials.

1. Synthesis of Zeolite Nanocrystals

1.1. Synthesis of Zeolite Nanocrystals from Clear Solutions and Gels. In a closed nutrient pool the increase of the number of viable nuclei leads to a reduction of the ultimate crystal size. Thus, the formation of zeolite nanocrystals requires conditions that favor nucleation over crystal growth in the system. Further, the zeolite nanocrystals have to be recovered with minimum aggregation if the purpose is stabilization of a colloidal suspension. The synthesized zeolite suspensions are usually purified by repeated high-speed centrifugation and redispersion in a liquid in an ultrasonic bath. The crystal size distributions are often obtained by at least two characterization techniques, one that is giving the average particle size, e.g., dynamic light scattering (DLS) and X-ray diffraction (XRD) from the XRD peak broadening using the Scherrer's equation, and another one that allows visual measurement of the particle size but represents a limited number of particles, scanning electron microscopy (SEM) and transmission electron microscopy (TEM). Most of the syntheses of zeolite nanocrystals have been performed using clear homogeneous solutions where only subcolloidal or discrete amorphous particles are present. This synthesis approach provides colloidal suspensions of discrete zeolite particles, often with sizes below 100 nm and narrow particle size distributions. High supersaturation and steric stabilization of the proto-nuclei are the key factors for the formation of nonaggregated zeolite nanocrystals. These conditions are usually achieved by the utilization of abundant amounts of organic structure-directing agents, whereas the alkali cations content is very low to limit the aggregation of the negatively charged (alumino)silicate subcolloidal particles. The system may contain some alkali cations, which facilitate the crystal growth, but quaternary ammonium cations in their OH^- forms usually play the structure-directing role and provide the high alkalinity needed for the synthesis. Further, relatively low crystallization temperatures are usually employed to minimize the ultimate crystal sizes. Lower temperatures favor the nucleation since the activation energy needed for crystal growth is generally higher.[5,6] All these factors together with a careful choice of the reactants and synthesis formulations allow the stabilization of clear solutions where only very small discrete amorphous particles are present.

Initial gel systems can also yield small crystals where the size of the individual crystals is in the order of nanometers. However, the crystals from such syntheses typically form aggregates of larger size and broad particle size distributions. The suspensions prepared from such products often do not possess the characteristics of typical colloidal suspensions as they tend to sediment. The preparation of zeolite particles of nanometric size with narrow particle size distributions from hydrogel precursors requires the utilization of highly reactive and uniform precursors. Besides the abundant and uniform distribution of nuclei, the processes of dissolution-recrystallization in such systems have to be minimized to provide products with narrow particle size distributions. Thus, initial solutions containing monomeric and/or low-mass silica and alumina species are used for the preparation of aluminosilicate gels.[7] These solutions are prepared by the following: (i) the utilization of easily dissolvable silica and alumina sources; (ii) the application of alkali bases in amounts sufficient to cause complete dissolution of the silica and alumina sources; and (iii) vigorous mixing, often at temperatures close to 0 °C, of the precursor solutions in order to form a synthesis mixture with homogeneous distribution of the components in the starting system. Similarly to clear solutions syntheses, the crystallization temperature is usually moderate to favor the nucleation over the growth in the system.

Syntheses of different zeolite structure types prepared in nanosized form from clear solutions and gels are summarized in Table 1.

1.1.1. Low and Intermediate Si/Al Zeolites (Types LTA, FAU, SOD, GIS, OFF, LTL, MOR, ZSM-2). Colloidal zeolite suspensions of LTA- and FAU-type zeolites have been prepared from diluted clear solutions containing a large amount of tetramethylammonium cations at temperatures from room temperature (22 °C) to 130 °C.[9−11,14−20] The yield of the syntheses was, however, often very low, ca. 10%. The presence of sodium in the synthesis mixtures for the synthesis of LTA- and FAU-type zeolites is essential since the large amount of framework Al cannot be compensated only by the bulky TMA^+ cation. The sodium concentration in the starting mixture was found crucial for the zeolite phase being crystallized, type LTA or FAU.[9,10,16,17] Higher sodium contents in the synthesis mixture resulted in shorter crystallization times and higher yields. Midsynthesis addition of sodium was used to obtain zeolite Y at Na_2O/Al_2O_3 levels that otherwise favored the crystallization of zeolite A.[16,17] It was found that the time at which the sodium is introduced into the crystallizing system should be after completion of the nucleation process. The midsynthesis addition of sodium was also used to increase the yield of zeolite Y and yields of more than 50% were achieved. The addition of 15-Crown-5 to the reaction mixture was studied in an attempt to broaden the SiO_2/Al_2O_3 ratios at which nanocrystals with FAU-type structure could be synthesized.[10] Although no such effect was observed, the authors found that the particle size distributions of the FAU-type crystals prepared in the

Table 1. Molecular Sieve Types Synthesized in Nanosized Form, Synthesis Conditions, and Crystal Size Ranges[a]

molecular sieve type	molar composition of the clear synthesis solution (S) or gel (G)	temp, °C	crystal size range, nm	ref
FAU	$5.5Na_2O:1.0Al_2O_3:4.0SiO_2:190H_2O$ (G)	60	20−100	8
LTA	$2.0-2.3(TMA)_2O:0.2-0.5Na_2O:Al_2O_3:3.4SiO_2:370H_2O$ (S)	100	230−240	9
	$1.2(TMA)_2O:0.42Na_2O:Al_2O_3:3.62SiO_2:246H_2O$ (S)			
FAU	$2.46(TMA)_2O:0.04Na_2O:Al_2O_3:3.4SiO_2:370H_2O$ (S)	100	100	9
	$1.576(TMA)_2O:0.044Na_2O:Al_2O_3:3.62SiO_2:246H_2O$ (S)			
FAU	$0.15Na_2O:5.5(TMA)_2O:2.3Al_2O_3:10SiO_2:570H_2O$ (S)	100	40−80	10,11
LTA	$1.12-3.6SiO_2:1.0Al_2O_3:1.5-7(TMA)_2O:0.007-0.28NaCl:276-500H_2O$ (G)	100	50+130−900	12
FAU	$3.4SiO_2:0.83-1.7Al_2O_3:2.3(TMA)_2O:0.1NaCl:300H_2O$ (G)	100	80	12
FAU	$4Na_2O:0.2Al_2O_3:1.0SiO_2:200H_2O$ (G)	25	100−300	13
FAU	$1.00Al_2O_3:4.35SiO_2:1.40-3.13(TMA)_2O(2OH^-):0-2.40(TMA)_2O(2Br^-):$ $0.048Na_2O:249.00H_2O$ (S)	100	32−120	14,15
FAU	$2.46(TMA)_2O:0.032-0.43Na_2O:1.0Al_2O_3:3.40SiO_2:370H_2O:13.6EtOH$ (S)	100,130, 100+130	75−137	16,17
LTA	$6.1-15.8SiO_2:Al_2O_3:17Na_2O:0.9-6.5(TMA)_2O:389H_2O:3^iPrO_2$ (∼S)	80	50−100	18
LTA	$0.3Na_2O:11.25SiO_2:1.8Al_2O_3:13.4(TMA)_2O:700H_2O$ (S)	22	40−80	19
LTA	$0.22Na_2O:5.0SiO_2:Al_2O_3:8.0(TMA)_2O:400H_2O$ (S)	63	130	20
SOD	$14(TMA)_2O:0.85Na_2O:1.0Al_2O_3:40SiO_2:805H_2O$ (S)	100	37	21
ZSM-2	$1.52(TMA)_2$ $O:0.53Li_2O:0-0.08Na_2O:3.4SiO_2:315H_2O$ (S)	100	49−108	22
GIS	$1Al_2O_3:4.17SiO_2:2.39(TMA)_2O:253H_2O$ (S)	100	30−50	23
OFF	$2.78(TMA)_2O:0.47-0.98K_2O:0-0.5Na_2O:Al_2O_3:9.90H_2O:91H_2O$ (n.s.)	85	45−60	24,25
OFF	$10SiO_2:1.0Al_2O_3:110-220H_2O:0.12Na_2O:0.5K_2O:3-4.5(TMA)_2O$ (G)	100	30−250	26
MOR	$6Na_2O:2Al_2O_3:30SiO_2:780H_2O$+seeds (G)	150	63	27
LTL	$10-12.5K_2O:1.0Al_2O_3:16-40SiO_2:250-450H_2O$ (S)	140−190	30−70	28
LTL	$10K_2O:1Al_2O_3:20SiO_2:400H_2O$ (S)	175	50−60	29
LTL	$8.0K_2O:Al_2O_3:20SiO_2:200H_2O$ (n. s.)	72.5,82.5,92.5	30−75	30
LTL	$0.005BaO:0.25K_2O:0.08Al_2O_3:1.0SiO_2:15H_2O$ (G)	170	140	31
BEA	$Al_2O_3:16-400SiO_2:5.16-105(TEA)_2O:240-6400H_2O$ (G)	140	10−200	32,33
BEA	$0.48Na_2O:9TEAOH:0.25Al_2O_3:25SiO_2:295H_2O$ (S)	100	60	34
BEA	$SiO_2:0.2(TEA)_2O:11.8H_2O$ (S)	100	100	35
MFI	$5-9TPAOH:0-0.3Na_2O:25SiO_2:0-0.25Al_2O_3:480-1500H_2O$ (S)	98	130−230	36
MFI	$1Al_2O_3:60SiO_2:21.4TPAOH:650H_2O$ (S)	170	10−100	37
MFI	$9TPAOH:0.16Na_2O:1Al_2O_3:50Si:300-495H_2O:0/100EtOH$ (S)	165	15−60	38
MFI	$Al_2O_3:60SiO_2:11TPAOH:900H_2O$ (S)	70,90	10−20	39
MFI	$0/0.53Na_2O:0.62-1.52(TPA)_2O:10SiO_2:60/143H_2O$ (S)	50,60, 80	25−80	40,24
MFI	$9TPAOH:0/0.1Na_2O:25SiO_2:480/1500H_2O:100EtOH$ (S)	98	95−180	41,42
MFI	$0.01-0.443TPAOH:20-80H_2O$:TEOS (S)	115	>90	43
MFI	$9TPAOH:25SiO_2:480H_2O:100EtOH$ (S)	60,80,60+100, 80+100	60−80	44
MFI	$3-13TPAOH:25SiO_2:480H_2O:100EtOH$ (S)	95	≥100	45
MFI	$3.0/4.5/9.0TPAOH:16NaOH:50SiO_2:495/2000H_2O:100EtOH$ (S)	60−98,165	20−1000	46
MFI	0.27Na2O:5TPAOH:25SiO2:420H2O (S)	22+230	130−260	47
MFI	$9TPAOH:25SiO_2:0.13Na2O:595H_2O:100EtOH$ (S)	60,100	60−170,100−300	48
MFI	9TPAOH:25SiO2:0.13Na2O:595H2O:100EtOH (S)	22+60,22+100	55−160,70−230	49
MEL	$0.55Na_2O:1.26(TBA)_2O:10SiO_2:150H_2O$ (S)	67.5,90	50−200	40
MEL	$SiO_2:0.3TBAOH:4.0EtOH:18H_2O$ (S)	22+100	90	50
MEL	$0.35TBAOH:1.0TEOS:12H_2O$ (S)	60−90	114	51
MFI	$9TPAOH:0.25TiO_2:25SiO_2:404H_2O:100EtOH$ (S)	100	85	52
MFI	$0.36TPAOH:0.06TiO_2:1.00SiO_2:16.2H_2O:4EtOH:0.24BuOH$ (S)	22+175(mw)	<100	53,54
AFI	$0.7-1.1(TEA)_2O:0.6-1.0Al_2O_3:1.1P_2O_5:50H_2O$ (G)	160, 150−160(mw)	50−300	55
AFI	$1(TEA)_2O:1Al_2O_3:1.32P_2O_5:110H_2O$ (G)	90,110,160(mw)	80−600	56
AEL	$1.6i\text{-}Pr_2NH:1.3-1.73P_2O_5:1.1Al_2O_3:35/70H_2O:0/0.8-1.2HF$ (G)	160,200	100−800	57
AEI	1Al2O3:3.16P2O5:3.16(TEA)2O:186H2O (S)	100,150,170	120−240	58

[a] Note: n.s., nonspecified; mw, microwave heating.

presence of 15-Crown-5 were narrower compared to those in the experiments performed in the absence of the co-template. Further, the size of zeolite Y nanocrystals has been minimized and the yield has been increased by using TMABr together with TMAOH as an additional source of organic template.[14,15]

The synthesis of LTA- and FAU-type nanocrystals from gel systems in the presence[12] or in the absence[8,13] of organic templates has also been reported. Zhu et al. used pure reactants and optimized synthesis conditions to obtain nano-LTA- and FAU-type crystals.[12] They used NaCl instead of NaOH as a sodium source; thus, the alkalinity of the reaction system was controlled only by the amount of TMAOH. It was found that when the $(TMA)_2O/Al_2O_3$ ratio was increased, the size of the LTA-type crystals decreased and that decreasing the amount of NaCl results in FAU-type crystals with low yield and low crystallinity. The synthesis of FAU-type crystals in the absence of organic additives has been performed by hydrothermal treatment at 60 °C.[8] The size of the NaX crystals was dependent on the silicate source, crystallization temperature, and agitation. The synthesis of FAU-type crystals from gel systems at ambient conditions that yielded 100−300 nm crystal aggregates built of 10−20 nm nanocrystals was reported as well.[13]

A method not listed in Table 1 that allows the synthesis of aggregated 30−40 nm particles of zeolite A by using a nonionic surfactant and poly(ethylene glycol) was recently described.[59] The growth of the zeolite precursors was

inhibited by the organic additives and by the ethylene oxide segments of the surfactant in particular, and the size of the primary zeolite A particles was nearly the same as the size of the aluminosilicate precursor species.

Other zeolites of the type SOD, GIS, ZSM-2, and OFF have been synthesized from clear synthesis mixtures or gels containing a large amount of TMA cations.[21−23,26] The synthesis of mordenite nanocrystals has also been reported.[27] However, this synthesis was possible only in the presence of seeds.

LTL-type zeolite nanocrystals have been synthesized from potassium hydroxide-containing systems in the absence of organic additives.[28−31] Meng et al. have synthesized ultrafine zeolite L powders with crystal sizes in the range 30−70 nm by optimizing the SiO_2/Al_2O_3, H_2O/Al_2O_3, and K_2O_3/Al_2O_3 ratios as well as the crystallization temperature.[28] Using a similar synthesis solution composition, Tsapatsis et al. synthesized zeolite L nanocrystals with a size of ca. 60 nm.[29] They found that the initially clear solution turned gelatinous early in the crystallization process and the gel gradually collapsed to a suspension. The zeolite L nanoclusters in their mother liquid started to settle when stored, indicating aggregation, but colloidally stable suspensions were obtained after purification. Zeolite L nanoparticles have also been synthesized from gel systems in the presence of a small amount of barium cations, which is a well-known structure-directing agent governing the formation of the LTL-type structure.[31]

1.1.2. High Si/Al Zeolites (Types BEA and MFI). Nanocrystalline zeolite Beta (type BEA) with a yield of up to 17% has been synthesized in the 8−200 range of initial Si/Al molar ratios from fluid gel systems containing TEAOH in the absence of alkali metal cations.[32,33] Fully crystalline samples with Si/Al ratios as low as 7.4 were synthesized. The output of all syntheses performed was a colloidal suspension of the zeolite in its mother liquor showing very low sedimentation rates. A decrease in the crystal size with increased Al content in the gel was observed coupled with a large increase in the external surface area.

Colloidal zeolite Beta suspensions have also been prepared from clear solutions in the presence of sodium and TEA cations.[34] It was found that the size of zeolite Beta was not affected by the alumina content in the initial solutions and that the time required to achieve the ultimate crystal size decreased with increasing alumina content. The increase of the sodium content resulted in an increase in the average crystal size and, similarly to previous results reported for FAU-type yielding precursor, reduced the crystallization time. Decreased water contents reduced the crystallization times and provided smaller crystals. The synthesis of purely siliceous nanocrystalline zeolite Beta in alkaline media from clear solutions has also been reported.[35]

ZSM-5 (type MFI) has been prepared in the form of stable colloidal suspensions from clear TPAOH-containing solutions.[36] It was found that the aluminum content did not affect the crystal growth rate but increase in the Al content resulted in a reduced number of crystals per gram of sol, smaller product yields, and an increase in the ultimate particle size. Decreasing the TPAOH content led to a large increase in the product yield and the crystal growth rate, whereas increased water contents resulted in larger crystals. Van Grieken et al. have reported the synthesis of nanocrystalline ZSM-5 by hydrothermal treatment of clear sodium-free synthesis mixtures at 170 °C with comparatively high yields, ca. 50%.[37] ZSM-5 aggregates with sizes in the range 100−200 and 400−600 nm composed of respectively 15 and 60 nm primary particles have been obtained from clear sodium-containing solutions at 165 °C.[38] ZSM-5 aggregates of 10−20 nm nanocrystals have also been obtained in the absence of sodium from clear solutions at 70−90 °C by a method based on the work of Van Grieken et al. with somewhat lower yields, 20−30%, related to the lower temperature used.[39]

1.1.3. Silica Molecular Sieves (Types MFI and MEL). Silicalite-1, the aluminum-free analogue of ZSM-5 (MFI structure type), is the most studied zeolite for the preparation of colloidal zeolite suspensions. The reasons are the simplicity of the system (no aluminum and alkali are present) and the properties of silicalite-1, e.g., hydrophobicity and high thermal stability. The synthesis conditions used by Persson et al.[41,42] have been adopted by many other research groups. The syntheses using the precursor solution from their work are highly reproducible and allow variations in the synthesis conditions, e.g., aging and heating, to prepare silicalite-1 crystals of decreased crystal sizes and improved yields. Upon hydrothermal treatment at 100 °C of the precursor clear solution of molar composition 9:25:480:100 TPAOH:SiO_2:H_2O:EtOH, colloidally stable suspensions containing discrete TPA-silicalite-1 crystals with an average size of 95 nm and narrow particle size distributions were obtained. Li et al. have developed a two-stage synthesis procedure consisting of a treatment at a lower temperature followed by a rapid change in temperature at some point during the course of the crystallization.[44] The initial temperature of the two-stage temperature procedure was maintained during the nucleation period and controlled the crystal population and the ultimate crystal size, whereas the higher temperature controlled the rate of linear growth of the crystals and the yield of silicalite-1. The procedure was used to improve the zeolite yield while minimizing the crystal size. For instance, the average crystal size of a one-step synthesis at 60 °C was 57 nm with a yield of 53%, whereas similar crystal sizes were obtained by a two-stage 60−100 °C procedure with a yield of ca. 60%, similar to yields obtained by the one-step procedure at 100 °C. Further, the authors studied the effect of the silica source and the aging on the crystallization of TPA-silicalite-1 using the two-stage varying-temperature procedure.[48,49] They found that nucleation was faster when TEOS was used as a silica source compared to the use of amorphous silica and the structure of the amorphous silica was of importance for the ultimate crystal size and concentration.[48] The crystal sizes when using TEOS were the smallest, e.g., 63 nm at 60 °C and increased to 160 and 169 nm when Ludox TM and Ludox LS, respectively, were used as silica sources. Similar trends were observed by Mintova and Valtchev.[60] Aging was found to increase the interaction between TPA^+ and the silica species, resulting in an increased structural ordering of the silica and units similar to those present in the crystalline

material were detected.[49] Crystal sizes, induction periods, and crystallization times decreased with aging. It was also found that with sufficient aging it was possible to substitute TEOS by the more economical Ludox silicas to obtain colloidal suspensions of similar quality. The effect of aging was employed by other authors to prepare colloidal silicalite-1 suspensions of reduced crystal size at higher temperatures. Cundy et al. found that, for aging times of up to 50 days, the product crystal size is sensitive to crystallization temperature and heating rate.[61] They tested temperatures of 90, 100, 150, and 175 °C (conventional heating) and 100 and 175 °C (microwave heating). After this aging time (50 days), the product size was independent of reaction temperature and type of heating. This was explained by the increased number of aging-generated proto-nuclei suppressing the normal self-nucleation of the reaction mixture. In another work, Cundy and Forrest added 5−20% 43 nm silicalite-1 seeds to the synthesis systems and found that the product crystal size decreased with an increase in the seed level and the final sizes were independent of the heating method, conventional or microwave.[62] Valtchev et al. used prolonged aging times (up to 60 days) and short hydrothermal treatment at 230 °C to obtain nanocrystals of silicalite-1 with well-developed crystal faces.[47]

Silicalite-2 (type MEL) is another purely silica molecular sieve that has been synthesized in colloidal form by hydrothermal treatment of diluted clear TBAOH-containing solutions at temperatures of less than 115 °C.[40,50,51] Thus, Mintova et al.[50] synthesized silicalite-2 crystals with an average size of about 100 nm, whereas Dong et al.[51] prepared 100 nm silicalite-2 aggregates composed of 20 nm crystals.

1.1.4. Titanosilicates and Aluminophosphates (Types MFI, AFI, AEL, AEI). Stable colloidal suspensions of TS-1 with average crystal sizes of less than 100 nm have been prepared by Zhang et al. with a maximum incorporation of Ti corresponding to 0.84 mol % Ti.[52] The presence of titanium in the precursor mixtures led to slower reaction kinetics. Dilution resulted in an increase in the crystal growth rate, the average crystal size, and the Ti content in the product. The Ti content in the product also increased with increasing temperature. The crystallization of titanosilicalite-1 from aged clear solutions at 175 °C (microwave heating) has been studied by Cundy et al.[53,54] They observed longer crystallization times with increasing titanium content and higher levels of framework titanium substitution at higher temperatures as well. In addition, similarly to silicalite-1, the particle size of TS-1 decreased with increasing aging time.

Nanometer-sized aluminophosphate molecular sieves with the AFI structure type have been synthesized from nearly transparent homogeneous gels using microwave heating.[55,56] However, particle size distributions for the products were broader. Nanocrystals of $AlPO_4$-11 (500 × 800 nm) have been synthesized from gel systems with conventional heating.[57] Colloidal suspensions of $AlPO_4$-18 with relatively narrow particle size distributions have been prepared from aged clear solutions at different temperatures.[58]

1.2. Confined-Space Synthesis of Zeolite Nanocrystals. Syntheses within an inert matrix providing a steric hindered space for zeolite crystal growth have been developed for preparation of zeolite nanocrystals. A schematic illustration of the confined-space procedures used for the synthesis of zeolite nanocrystals is given in Figure 2. The first example of such a synthesis was reported by Madsen and Jacobsen for the preparation of nanosized ZSM-5 crystals.[63] The synthesis procedure consisted of incipient wetness impregnation of mesoporous carbon black with clear solutions containing TPAOH, distilled water, ethanol, and alumina, subsequent impregnation with TEOS, transfer of the impregnated matrix into a porcelain cup, and treatment in an autoclave with sufficient water to provide saturated steam at 180 °C. Detailed studies on the properties of the ZSM-5 crystals as well as of features of other zeolites such as Beta, X, and A prepared using this procedure have been performed.[64,65] Two carbon black matrixes were used with a pore diameter of 31.6 and 45.6 nm, respectively. Generally, the crystal size distributions of the zeolites obtained were governed by the pore size of the carbon black matrix and were typically in the range 30−45 nm. Unlike colloidal zeolites, the recovery of the nanozeolites prepared can be easily realized by simple calcination, during which both the carbon matrix and the zeolite structure-directing templates are removed. The mesopore volumes of the carbon black templates used resulted in more than 10 wt % of zeolite in the final product. Crucial steps in the synthesis were (i) restriction of the crystallization of the zeolite gel within the pore system of the matrix, which was achieved by the incipient wetness impregnation method employed to load the mesopores with a synthesis gel, and (ii) prevention of diffusion of the zeolite gel species from the mesopores, which was ensured by avoiding direct contact between the impregnated carbon black matrix and the water at the bottom of the autoclave. Drawbacks of the method are the requirements imposed on the matrix to be used as a confined-space media, namely, inertness and stability under the experimental conditions and sharp mesopore size distribution to yield uniform crystal size distribution of the zeolite crystallized inside.

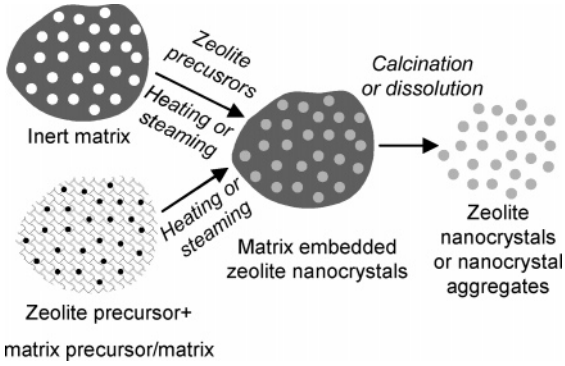

Figure 2. Scheme for the confined-space syntheses of zeolite nanocrystals.

Colloid-imprinted carbons with average pore sizes of 12, 22, 45, and 85 nm have been used as confinement templates for the synthesis of ZSM-5 zeolite crystals with highly uniform crystal size distributions and average sizes close to that of the template pores, 13, 22, 42, and 90 nm, respectively.[66] The zeolite nanocrystals obtained upon calcination were intergrown into larger aggregates, which can be beneficial for catalytic applications. Also, the aggregates can

easily be recovered from liquid suspensions by filtration. Hard aggregates composed of ca. 20 nm ZSM-5 crystals have also been prepared using a surfactant as an inert matrix for the zeolite crystal growth.[67] In this study, dried zeolite precursor/surfactant hybrids were pressed into pellets and converted into a zeolite by steaming in an autoclave, whereas the organic components were removed by calcination. Later, the authors reported on an improved synthesis scheme so that nanocrystals with a size of 10−20 nm were obtained.[68] When those nanocrystals were dispersed and sonicated in an ammoniac-ethanol solution, the nanocrystals self-assembled into hollow spheres of 100−300 nm diameter. The confinement effect of carbon nanotubes for the synthesis of zeolite Beta nanocrystals has also been reported.[69] The authors synthesized zeolite Beta inside multiwalled carbon nanotubes with an average diameter between 50 and 80 nm in the form of zeolite nanowires composed of 10 nm particles. However, the material was XRD amorphous, which was attributed to the small crystal size.

Other examples of confined-space synthesis, though resulting in zeolites with broader crystal size distributions, have been reported.[70,71] Those syntheses were performed in the absence of organic structure-directing agents and yielded smaller zeolite crystals compared to syntheses performed in the absence of space-confinement additives. Zeolite NaY with a size in the range 50−100 nm has been synthesized using starch as a matrix.[70] However, calcination was necessary to remove the starch template. An elegant calcination-free approach has been used by Wang et al. for the synthesis of NaA (20−180 nm) and NaX (10−100 nm) nanocrystals employing thermoreversible polymer hydrogels to space limit the crystal growth.[71] The zeolite crystals obtained were recovered from the polymer matrix by simple cooling of the mixture and washing away of the water-soluble polymer.

2. Zeolite Precursor Solutions or Gels Yielding Nanocrystals as Model Systems for Studying Zeolite Crystallization

Zeolite formation is still not well understood, except in that it appears that there is no single universal mechanism to describe all zeolite syntheses. The two extremes of the proposed mechanisms of zeolite formation are as follows: (i) solution-mediated transport mechanism and (ii) solid hydrogel transformation mechanism. In any particular reaction system the true mechanism could lie somewhere between these two extremes. In the next two sections, the insights into crystallization mechanisms achieved using nanocrystal-yielding solutions or gels as model systems will be reviewed.

2.1. Clear Solutions. It is clear now that the crystals obtained from solutions are often not formed via classical pathways but by much more complex routes.[72] This conclusion is particularly true for zeolite yielding systems where the reaction media are in general inhomogeneous and zeolite nucleation and crystal growth involve numerous simultaneous equilibria and condensation steps. Consequently, the efforts for a detailed understanding of phenomena governing zeolite crystallization go on in order to reach the ultimate goal, i.e., a rational control of the synthesis of these materials.

The systems yielding zeolite nanocrystals were found very useful for investigations on zeolite crystallization. In general, the crystallization of such nanocrystals is performed from clear solutions where only discrete amorphous particles are present. Contrary to the conventional gel systems, where a large diversity of (alumino)silicates species is usually present, the initially clear solutions contain a limited number of well-defined discrete amorphous precursor particles. Therefore, the investigations based on such systems facilitate the interpretation of the results and ambiguous conclusions will be avoided. It should be recalled also that the synthesis of zeolite nanocrystals is usually performed at relatively low crystallization temperatures which makes in situ studies possible without using very complicated equipment. This is particularly important for investigations on the nature of the very small labile subcolloidal particles that are present in the very first stages of zeolite formation.

Schoeman[73] first revealed the homogeneous nature of such precursor systems and showed that the system typically used for the synthesis of colloidal silicalite-1 crystals ($9TPAOH:25SiO_2:480H_2O:100EtOH$) contains ca. 84 wt % of the silica in the form of polymeric species with an average particle size of 2.8 nm. The analysis was based on the reaction of monomeric silica species with molybdic acid and the results agreed with previous DLS and cryo-TEM investigations.[74] Further, the investigation of such a system showed that the subcolloidal particles possess a short-range order. Thus, the presence of absorption bands characteristic of double-ring units that could be attributed to the MFI-type structure was detected in the DRIFT spectra of the extracted powder.[75] The fact that the 2.8 nm particles comprise an organic structure-directing agent (tetrapropylammonium) was proved by Watson et al.[76] using a combination of small-angle X-ray (SAXS) and neutron scattering (SANS) and IR spectroscopy. Thus, the silicalite-1 clear precursor solution was found very appropriate as a model system for studying the zeolite formation of the zeolite. Numerous investigations aiming at shedding more light on the zeolite nucleation/crystallization process were performed on similar systems. Initial systems and major techniques employed in these studies and the corresponding references are summarized in Table 2.

All researchers agreed on the fact that the silicalite-1 precursor solution formed by hydrolysis of tetraethylorthoslicate in a TPAOH-containing solution under ambient conditions comprises discrete particles with a size of about 3 nm. The ongoing discussion is how these proto entities are transformed into silicalite-1 crystals. According to the model proposed by Schoeman, a cluster−cluster aggregation mechanism is dominating until a certain size is reached (ca. 1 nm) and after that the growth mechanism is via deposition of low molecular weight species on to growing crystals.[82] Based on the extended Derjaguin-Landau and Verwey-Overbeek (DLVO) theory, he suggested that it is not likely that silicalite-1 crystals grow via a particle−particle aggregation mechanism. However, by analyzing a similar system, Watson et al.[80] came to a diametrically opposite conclusion. According to their model, the colloidal particles formed in the initial solution already possess the typical

Table 2. Initial Systems, Experimental Conditions, Major Techniques, and References of the Investigations Devoted to Silicalite-1 Formation from Clear Homogeneous Solutions

initial system	characterization technique[a]	conditions	ref
$9TPAOH:Na_2O:25SiO_2:450H_2O$	DLS	in situ	77
$9TPAOH:25SiO_2:480H_2O$:100EtOH	cryo-TEM, DLS	ex situ	74
$9TPAOH:25SiO_2:480H_2O$:100EtOH	molybdate method	in situ	73
$9TPAOH:25SiO_2:480H_2O$:100EtOH	Raman, IR spectroscopy	ex situ	75
$9TPAOH:25SiO_2:480H_2O$:100EtOH	DLS	in situ	78
$3.125TPAOH:25SiO_2:350-390H_2O$	SAXS, WAXS, IR, SEM, TEM	ex situ	79
$0.12TPABr:0.297Na_2O:1.0SiO_2:120H_2O$	SAXS, SANS, DLS	in situ + ex situ	80
$0.4-0.8Na_2O:1.2(TPA)_2:10SiO_2:117H_2O$	synchrotron SAXS−WAXS	in situ	81
$9TPAOH:0.1Na_2O:25SiO_2:480H_2O$:100EtOH	theoretical study		82
$0.297Na_2O:0.12TPABr:1.0SiO_2:120.0H_2O$	SAXS, SANS, IR,	in situ + ex situ	76
$9TPAOH:25SiO_2:480H_2O$:100EtOH	DLS, SEM	ex situ	44
$0.4-0.8Na_2O:1.2(TPA)_2:10SiO_2:117H_2O$	SAXS−WAXS, USAXS	in situ	83
$9TPAOH:25SiO_2:480H_2O$:100EtOH	XRD, SEM, TEM, 29Si NMR, TG, IR, N2 adsorption	ex situ	84
$9TPAOH:25SiO_2:480H_2O$:100EtOH	TG, IR, UV−Vis, 13C NMR	ex situ	85
$9TPAOH:25SiO_2:480H_2O$:100EtOH	SAXS, TEM, 29Si NMR, AFM	ex situ	86
$9TPAOH:25SiO_2:480H_2O$:100EtOH	29Si NMR, IR	in situ + ex situ	87
$9TPAOH:25SiO_2:480H_2O$:100EtOH	XRS, GPC	in situ + ex situ	88
$9TPAOH:25SiO_2:480H_2O$:100EtOH	XRD, theoretical study	ex situ	89
$9TPAOH:25SiO_2:480H_2O$:100EtOH	GPC, IR	ex situ	90
$1.0NaOH:2.4TPAOH:10.0SiO_2:110H_2O$	DLS, AFM, modeling	ex situ	91
$21.4TPAOH:Al_2O_3:60SiO_2:650H_2O$	XRD, TEM, NMR, X-ray fluorescence, N2 adsorption	ex situ	37
1.0(TPA)2O:3.75SiO2:30.0H2O15.0EtOH	DLS, SAXS, TEM, 29Si NMR,	ex situ	92
$9TPAOH:25SiO_2:530H_2O$:100EtOH	DLS, TEM, XRD, 29Si NMR	ex situ	93
$1.0TPAOH:2.7TEOS:16.0H_2O$	29Si liquid NMR	in situ	94
$9TPAOH:25SiO_2:480H_2O$:100EtOH	calorimetry/pH measurements	in situ	95
$9TPAOH:25SiO_2:480H_2O$:100EtOH	XRD, IR, NMR, TG, N2 adsorption, modeling	ex situ	96
$9TPAOH:25SiO_2:480H_2O$:100EtOH	calorimetry/pH measurements, potentiometry, SAXS	in situ	45
$9TPAOH:25SiO_2:480H_2O$:100EtOH	TEM, EDX, AFM	ex situ	97

features of the MFI framework geometry. During the induction period these primary nuclei fuse coaxially, yielding the primary crystallites with an average length and diameter of 33 and 8.3 nm, respectively. Further growth takes place by a fusion of the primary crystallites.

The largest work on the mechanism of silicalite-1 crystallization from a clear solution was performed by the group from Leuven.[84−90,92,94] A number of complementary techniques were used to follow the entire process of silicalite-1 formation. ^{29}Si liquid NMR and in situ infrared spectroscopy were employed to study the nature of the precursor species in the silicalite-1 yielding solution. The conclusion of this investigation is that under ambient conditions the polycondensation process leads to the selective formation of a species containing 33 Si atoms (Figure 3, part A). These species occlude TPA cations and possess the MFI-type framework features, which is in agreement with the first stage of the model proposed by Watson et al.[80] The size of these primary units, called nanoslabs, is 1.3 × 4 × 4 nm, where the large 4 × 4 nm surface is perpendicular to *a*. According to this model already at room temperature these sheets are linked via the small sides in the *b* and *c* direction and thus 2 × 2 sheets are formed. Further aggregation at room temperature is energetically unfavorable and only a rise of the temperature can promote the growth (Figure 3, part B). This model is without any doubt the most detailed and accomplished one. However, some later findings are in serious disagreement with the nucleation/crystallization scenario proposed by the Leuven group.[96−98] Thus, the discussion on the formation of silicalite-1 does not seem to be closed.

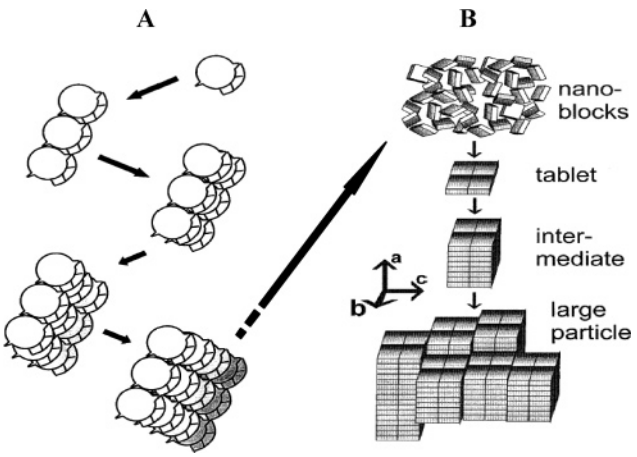

Figure 3. Proposed mechanism of (A) nanoslab formation and (B) silicalite-1 crystal growth by aggregation of nanoslabs. Redrawn with permission from refs 88 and 89, respectively.

The localization of the viable zeolite nuclei, which promote crystallization, is an important issue that could shed light on subsequent events in the process of zeolite crystallization. Subotic et al.[99,100] developed the "autocatalytic nucleation" model in which nuclei liberated during the dissolution of the gel phase promote zeolite crystallization. Further development of this model revealed that it can be applied successfully only to nuclei that are located near the outer surface of the gel particles.[101,102] The crystallization mechanism of FAU-type nanocrystals obtained from a clear solution was somewhat different from the accepted one for conventional gel systems.[11] It was found that the initial system yielding FAU-type material contained distinct 25−35 nm amorphous particles. Each amorphous aggregate nucleated only one single zeolite crystal, with the nucleation always starting at the gel−solution interface (Figure 4a). The nuclei did not leave the amorphous gel particles; instead, a progressive transformation of the gel into crystalline material was observed and the FAU-type structure which emerged in the peripheric part invaded the entire volume of the precursor particle.

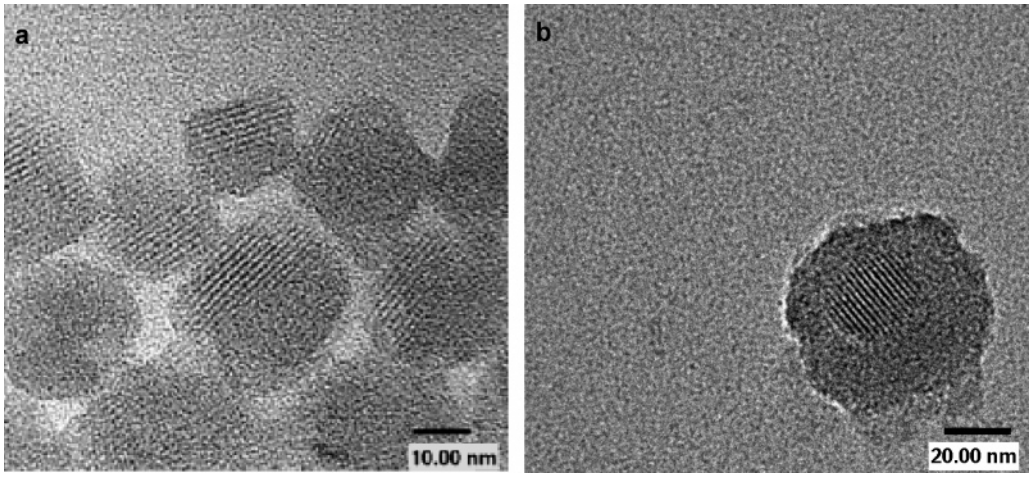

Figure 4. TEM images of lattice fringes of FAU- (a) and LTA- (b) type zeolites emerging within the amorphous precursor particles. Copied with permission from refs 11 and 19, respectively.

Regarding the formation of MFI- and FAU-type zeolites from clear solutions, there is a diversity of pathways for both the nucleation and crystal growth reactions. Although both systems look fairly similar, i.e., clear homogeneous solutions, the nucleation/crystallization mechanisms are completely different. The formation of MFI-type materials goes through formation of colloidal (∼3 nm) particles that grow either via the addition of low weight silica species or via aggregation. The precursors of FAU-type zeolite are colloidal particles (25−35 nm), which maintain their size during the crystallization process, as was discussed above.

2.2. Ambient Synthesis of Zeolite Nanocrystals and Their Use for the Investigation of the Mechanism of Zeolite Formation. Generally, the zeolite syntheses are performed in the temperature range 90−200 °C for periods of time between several hours and several weeks.[103,104] It is well-known, however, that the aging under ambient conditions has a pronounced effect on the subsequent crystallization process. Several groups suggested that the aging step results in the formation of viable nuclei, which induce the crystallization when the temperature is raised.[105−107] If zeolite nuclei are formed under ambient conditions, there are neither thermodynamic nor chemical considerations that do not allow further growth of the crystallites. However, as can be expected, the kinetics of such a crystallization process is relatively slow. Indeed, geological time is needed for the formation of natural zeolites at low temperatures in closed alkaline and saline-lake systems.[108] However, there are a few examples showing the feasibility of ambient temperature synthesis of aluminosilicate zeolites on a laboratory time scale. For instance, after 47 days of aging at ambient conditions, a liquid-free gel was partially (ca. 20%) converted into zeolite X.[103] Using a conventional organic template-free $Na_2O-Al_2O_3-SiO_2-H_2O$ system, Sand et al.[109] synthesized zeolite A with a crystallinity of about 70−80% after 28 days at room temperature. The long duration of these syntheses and partial transformation of the initial gel into a zeolite make them not very useful for practical applications. A substantial reduction of the synthesis time combined with full conversion of the initial system into a zeolite-type material at room-temperature conditions would make such syntheses very useful from an academic point of view since they might be used for the investigation of the mechanism of zeolite formation. The sluggish crystal growth kinetics at ambient conditions would permit tracking down of the entire sequence of crystallization events from the formation of the initial gel to the complete transformation into a zeolite-type material.

Thus, the formation of LTA-type crystals at room temperature (RT) from a system with the composition $0.3Na_2{:}11.25SiO_2{:}1.8Al_2O_3{:}13.4(TMA)_2O{:}700H_2O$ was followed by means of high-resolution transmission electron microscopy (HRTEM).[19] The investigation showed that the organic template, tetramethylammoinum (TMA), provokes the aggregation of the primary (5−10 nm) colloidal silica particles leading to the formation of 40−80 nm aggregates. The first XRD proof for the formation of LTA-type zeolite was recorded after 3 days of treatment at RT. HRTEM inspection revealed that the first crystallites with a size of 5−14 unit cells (10−30 nm) were embedded in the amorphous aggregates (Figure 4b). Each amorphous aggregate contained one nucleus, which progressively grew from the center of the particle outward. Thus, after 1 week of treatment at RT, the amorphous particles were completely converted into crystalline 40−80 nm LTA-type crystals. The high supersaturation within the gel particles is supposed to be the driving force for this type of zeolite nucleation. The fact that the amorphous particles maintained their average size over the course of complete conversion into denser zeolite structure supposes a supply of nutrients from the mother liquor.

Unlike the zeolite A crystal growth at RT, an interesting observation is that the emerging of the FAU-type structure synthesized at 100 °C was observed at the peripheric part (Figure 4a).[11] The major difference between these two systems is the temperatures used, RT or 100 °C. Therefore, the thermal gradient, the resultant convection streams, and all consequent changes in the system might be the reasons for the observed nucleation at the peripheric part of the precursor particles yielding FAU-type zeolite.

It is interesting to compare the formation of the same zeolite structure type from organic template-containing and

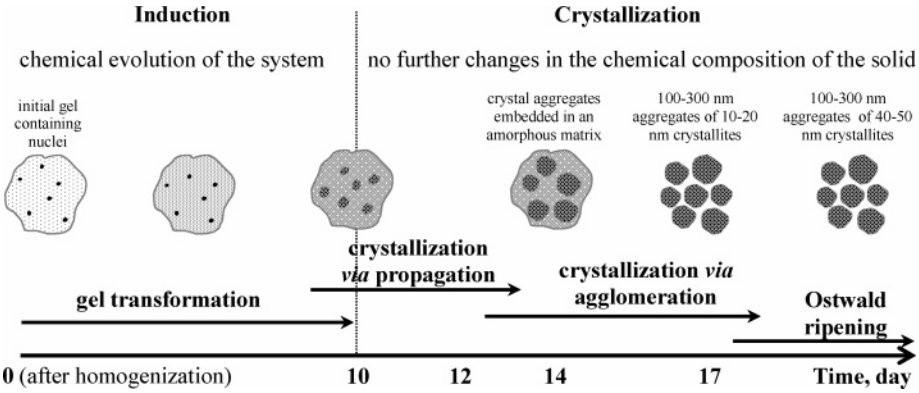

Figure 5. Schematic illustration of the crystallization mechanism of FAU-type zeolite under ambient conditions. Copied with permission from ref 13.

organic template-free systems. Very recently, the organic-free synthesis of FAU-type zeolite at room temperature was reported. The investigation was based on HRTEM complemented by in situ synchrotron X-ray powder diffraction (XRD) and ex situ laboratory techniques, e.g., XRD, IR, DLS, N_2 adsorption measurements, and chemical analysis.[13] The careful analysis of the system revealed a crystallization scenario different from those observed for FAU- and LTA-type materials obtained from low sodium and high TMA-containing systems.[11,19] The sodium in the system provoked abundant aggregation of polymerized aluminosilicate species resulting in a fairly open gel structure. It is worth mentioning that areas that are quite likely to be the places for zeolite nucleation were found in the gel structure. These parts of the gel called "negative crystals" represent faceted cavities filled with liquid inclusions trapped in the gel phase. Further, the structural and chemical evolutions of the system were tracked down and the nanometer-scale transformations studied by TEM were coupled with a set of complementary analyses which provided new insights into the mechanism of zeolite formation. The observed events are schematically presented in Figure 5. The main stages could be summarized as follows: (i) the system reaches a specific critical level of chemical evolution before the onset of crystallization; (ii) during the first crystallization stage (10−15% crystallinity), a crystal growth by propagation through the gel phase dominates; (iii) the second crystallization stage includes spontaneous aggregation of nanoparticles around a crystallization center followed by an Ostwald ripening. This crystallization mechanism provided 100−300 nm round-shaped aggregates built of FAU-type nanoparticles.

The above examples are a sound demonstration of the variety of zeolite crystallization mechanisms. FAU- and LTA-type possess similar structural features and often crystallize from systems with close compositions. Nevertheless, their formation proceeds via different crystallization routes depending on the initial composition and synthesis conditions employed. Different crystallization mechanisms were also observed during the formation of FAU-type materials synthesized in the presence and in the absence of organic template. Hence, the zeolite formation is far from being well understood and any new information is welcome.

3. Applications of Zeolite Nanocrystals

3.1. Preparation of Structured Materials Using Colloidal Zeolite Crystals. Zeolite nanocrystals and colloidal zeolite suspensions in particular are very convenient materials for the preparation of structured materials. With the term structured materials we denote polycrystalline extended zeolite structures, which have a certain level of organization. The organization could be on a macrolevel, i.e., their macro-morphological features, or on a nanolevel, where the spatial arrangement of the nanocrystals could provide materials with bi- or three-modal pore organization. Hierarchical porous materials with specific macro-morphological features, hollow, and supported zeolite structures will be revised.

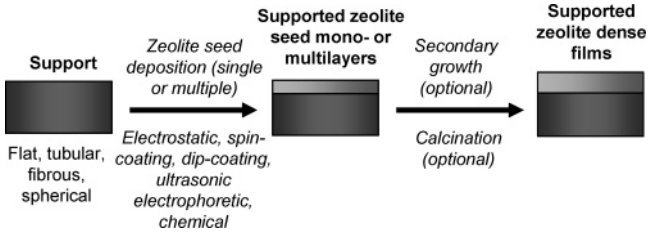

Figure 6. Schematic illustration of the methods for the preparation of supported zeolite films by seeding.

3.1.1. Supported Zeolite Films and Membranes. The use of preformed zeolite nanocrystals for the preparation of supported zeolite films and membranes is one of the major applications of colloidal zeolites. Generally, the quality of a zeolite coating on various supports is determined by the homogeneity and intactness of the zeolite layer and the number of defects in the film, such as cracks and pinholes. Largely used procedures to produce zeolite-supported layers of improved quality comprise a preliminary adsorption of zeolite nanoseeds, which are induced to grow into a dense film by secondary growth. To review the vast number of papers on preparation of zeolite films and membranes is beyond the objectives of the present review. A number of comprehensive reviews in this area have appeared recently.[110−116] Here, the methods for attaching zeolite colloidal seeds prior to preparation of supported zeolite layers will be listed. Schematically, those methods are illustrated in Figure 6. A very important feature of the zeolite film syntheses by seeding is that the preliminary adsorption of seeds may cause a preferred orientation of the growing zeolite crystals. This topic is well-covered by the review articles on membranes. In some cases, the support may be removed after the synthesis by combustion or dissolution and the zeolite structures obtained are self-standing. The self-standing zeolite structures are often characterized by a poor mechan-

ical stability. Therefore, such structures will rather be considered in this section than in the next one devoted to solely zeolitic materials unless they are conceptually interesting for preparation of the latter.

The first example of a procedure for attaching zeolite nanoseeds onto a support has been reported by Lovallo et al.[117] Zeolite L colloidal seeds were attached to the surface of a glass slide by repeated dipping of the support in alternating suspensions of boehmite and zeolite L having opposite surface charges. However, the presence of boehmite within the zeolite film may be a drawback for some applications, where pure zeolite coatings are needed. This has been overcome by the use of a polymeric binder to electrostatically adsorb zeolite seeds.[118] In this method, the substrate surface is first charge-modified by a cationic polymer; negatively charged colloidal zeolite crystals are then adsorbed and the seeds are subjected to a secondary growth by hydrothermal treatment with a fresh synthesis solution or gel. The polymer as well as the zeolite structure-directing agents are removed during a subsequent calcination. The seed-film method was also adopted for the preparation of zeolite films on gold supports by an additional step, namely, the initial adsorption of γ-mercaptopropyltrimethoxysilane followed by its hydrolysis in acidic media. This step was necessary to obtain a negative surface charge of the Au support to facilitate subsequent adsorption of either a cationic polymer[119] or positively charged silicalite-1 crystals obtained by treatment with a strongly acidic cation-exchange resin.[120] Zeolite seed crystals have also been spin-coated on flat supports but this method will be considered in detail in section 3.4.2.

Another method to obtain zeolite seed layers is by dip coating.[121,122] The supports were dipped three times in colloidal zeolite suspensions followed by drying at room temperature. Holmes et al. have deposited silicalite-1 seed crystals on a stainless steel mesh by sonication.[123] The authors placed the support in a jar together with a colloidal silicalite-1 sol and treated it ultrasonically for 6 h, during which time the temperature increased to ca. 70 °C. Electrophoretic deposition has been reported as another method to assemble nanozeolites onto supports.[124,125] The method has been applied using nanozeolites in both aqueous[124] and nonaqueous[125] media.

Kulak et al. have obtained monolayers of zeolite A and ZSM-5 on glass and mica by independent tethering of two different functional groups onto the zeolite and the substrate, followed by covalent linking of the two tethered functional groups.[126] This method was reported for micrometer-size crystals, but can be applied using nanozeolites as well. Another highly efficient and economical method of assembling zeolite crystals on glass supports has been developed by the same group.[127] 3-Halopropylsilyl reagents were used as covalent linkers and either the support or the zeolite crystals could be modified, but for simplicity reasons the authors preferred to modify the glass plates. Another example of chemically arranging colloidal nanoparticles is by the addition of hexanoic acid to the TS-1 suspension.[128] The acid is adsorbed on the dispersed zeolite particles and the substrate surface and the hydrophobic force in an aqueous medium is sufficient to cause the zeolite particles to deposit on the substrate as a thin film.

Finally, an example of a zeolite membrane preparation, illustrating how the knowledge gained by different groups can be combined to optimize the properties and the performance of the product membrane will be considered in this section. The siliceous ZSM-5 membrane prepared by Lai at al. showed high selectivity with excellent ability to separate *p*-xylene from *o*-xylene, the difference in size between the two being less than 0.1 nm, while maintaining high permeance.[129] The zeolite membrane was ca. 1 μm thick with the straight zeolite channels running down the membrane thickness and characterized by a very low defect density, meaning that the transport outside the zeolite pores was negligible. The three crucial points for achieving such a performance were as follows: (i) the α-alumina support used was first coated with a layer of amorphous silica using a sol−gel technique to provide a smooth surface for the subsequent seed deposition, to prevent zeolite crystallization within the support and to eliminate stress-induced crack formation during calcination; (ii) deposition of seed crystals with their *b* axis perpendicular to the support surface using the method developed in ref 127; and (iii) secondary growth of the seed layer using trimer-TPA template, which enhanced the relative growth along the *b* axis, thus preserving the *b*-orientation of the zeolite seed layer even after film thickening by secondary growth.

3.1.2. All-Zeolite Structures Synthesized by the Application of Zeolite Nanocrystals. The interest in preparing macroscopic zeolite structures is driven by the following: (i) the optimized zeolite performance (no pore blocking and zeolite diluting binding additives are present), easy handling, and attrition resistance; (ii) the presence of secondary larger pores that minimize diffusion limitations; and (iii) possibilities for nonconventional applications, such as guest encapsulation, bioseparation, enzyme immobilization, etc. Currently, the procedures used to prepare hierarchical zeolite structures are by use of sacrificial macrotemplates, molds, micropatterning, and self-assembly of nanocrystals. In the following sections, the different approaches for the preparation of all-zeolite macrostructures based on the use of either preformed zeolite nanocrystals or by in situ crystallization using solutions yielding colloidal zeolites will be reviewed.

Hollow Zeolite Spheres and Related 3D-Structures. Polystyrene spheres (PS) are among the most widely used templates for the fabrication of structured zeolites. They can be prepared in a variety of particle sizes, are able to self-assemble into periodic 3D-arrays, and can easily be removed when necessary by thermal or chemical treatment. The methods for the fabrication of hollow zeolite spheres or ordered macroporous zeolite macrostructures are schematically illustrated in Figure 7. A drawback is their low glass transition temperature, which limits the synthesis temperatures that can be used. Hollow zeolite spheres have been prepared employing polystyrene spheres and the layer-by-layer method.[130,131] In brief, alternating layers of oppositely charged polycations and preformed zeolite nanocrystals were adsorbed on the PS spheres to achieve the desired thickness of the zeolite layer and the PS template was finally removed

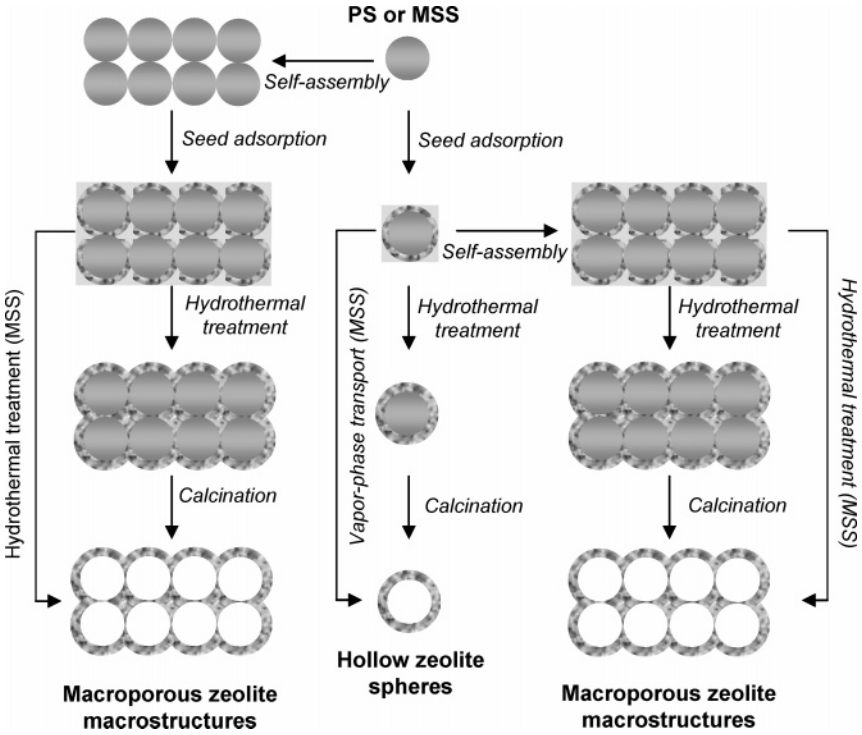

Figure 7. Schematic illustration of the methods for the fabrication of hollow zeolite spheres or ordered macroporous zeolite structures using polystyrene (PS) or mesoporous silica spheres (MSS).

by combustion. However, the mechanical stability of the obtained hollow zeolite spheres was low. Holland et al. have reported the first example of ordered macroporous zeolite macrostructures using PS templating.[132] In addition, this is the only report on the preparation of such structures in which in situ crystallization without the addition of seeds was employed. Thus, PS spheres were centrifuged to form close-packed arrays, which hardened in a solution containing TEOS and TPAOH, and upon hydrothermal treatment and calcination, a macroporous silicalite-1 composite formed with wall thicknesses in the range 20−220 nm. Macroporous zeolite macrostructures have also been obtained by arranging PS via suction filtration followed by the addition of preformed silicalite-1 crystals[133] or by depositing preformed zeolite crystals on PS by the layer-by-layer method and subsequent centrifugation to arrange the zeolite-coated PS into close-packed assemblies.[134]

The mechanical stability of hollow zeolite spheres synthesized by the layer-by-layer method could be improved by secondary hydrothermal treatment with synthesis gels or solutions of suitable compositions.[135,136] Secondary hydrothermal treatment has been applied to improve the strength of macroporous zeolite composites as well.[136,137] Those macrostructures were prepared by arranging zeolite-coated PS into 3D-arrays by sedimentation in a synthesis solution followed by hydrothermal treatment[136] or by mixing PS with colloidal zeolite suspensions and self-assembling by sedimentation followed by slow solvent evaporation and subsequent hydrothermal treatment with a fresh synthesis solution.[137]

Mesoporous silica spheres (MSS) have also been employed as a template to prepare zeolite monoliths of ordered closed macroporous.[138] In addition to being macropore-yielding templates, the MSS served as a silica nutrient for the zeolite formation. The method consisted of coating the MSS with preformed zeolite nanocrystals and arranging the coated MSS into a 3D-array by sedimentation into a clear synthesis solution followed by hydrothermal treatment, during which silica from the MSS was consumed. This procedure, except that the seeded MSS were transferred into a zeolite by the vapor-phase transport method, has also been applied to prepare hollow zeolite spheres.[139] The fact that the MSS are consumed during the synthesis has been employed to prepare guest-encapsulated hollow zeolite spheres or ordered macroporous monoliths.[139−141] In addition, mesoporous silica (MS) particles with various nonspherical shapes (gyroid, egg, discoid, and cakelike shapes) were used as starting materials and hollow zeolite structures with corresponding shapes were prepared in a similar way.[140] Metals (Ag),[140,141] metal oxides (Fe_2O_3, PdO),[139−141] carbon and polymer of micrometer size[141] were successfully encapsulated in the interiors of the hollow zeolite structures. The use of MS with a wormlike morphology as a template, which resulted in product hexagonal hollow ZSM-5 tubes, has also been reported.[142] Thus, silicalite-1 seeds were electrostatically assembled onto the MS and the seeded MS was impregnated with $Al(NO_3)_3$ and NaCl aqueous solutions to incorporate aluminum during the subsequent vapor-phase transport treatment. Recently, Wang and Caruso modified the synthesis procedure employing MSS to prepare 3D interconnected macroporous zeolitic membranes that can be used as supports for enzyme immobilization.[143] They assembled the MSS into a membrane by sedimentation and calcination; a zeolite layer was then seeded in the voids of the MSS membrane by electrostatic nanocrystal deposition followed by hydrothermal treatment with a synthesis solution.

Biological Macrotemplating. Biological species are excellent for serving as macrotemplates: they are inexpensive and

environmentally benign and provide thousands of possibilities for the synthesis of hierarchical structures. Thus, bacterial supercellular threads have been infiltrated with preformed zeolite nanoparticles to yield ordered macroporous zeolite fibers upon calcination.[144] Diatomite is another macrotemplate that has been used to produce hierarchical zeolite structures.[145−147] Diatomite is a sedimentary rock, composed of the fossilized skeletons of diatoms, one-celled algae-like plants which accumulate in marine or lacustrine environments. The honeycomb silica structures give diatomite useful characteristics such as high absorptive capacity and surface area, chemical stability, and low bulk density. The approaches used were as follows: (i) diatomite seeding with zeolite nanoparticles by sonication followed by hydrothermal treatment in a synthesis mixture;[145] (ii) diatomite seeding by electrostatic deposition[146,147] and subsequent vapor-phase transport treatment.[146] The zeolite Beta-diatomite composite prepared in ref 147 after ion-exchanging cobalt ions into the zeolite was found useful for the separation of histidine-containing polypeptides and proteins.

Hierarchical zeolite structures have also been prepared by wood cell templating.[148] Two kinds of tissues, cedar and bamboo, were covered with a thin layer of zeolite seeds by electrostatic adsorption of colloidal seeds, and upon secondary hydrothermal treatment and calcinations, a zeolitic tissue faithfully replicating the wood macrocellular structure was obtained. Another example of a preparation of biomimetic zeolite structures is by using *Equisetum arvense* as a macrotemplate.[149,150] *Equisetum arvense* is a plant rich in amorphous silica (10−13 wt %) deposited in discrete knobs and rosettes at the epidermal surface. The zeolite replication was realized by in situ crystallization employing clear synthesis solutions otherwise yielding colloidal zeolites without any pretreatment of the plant, the zeolitization being induced by the biogenic silica stored within its structure, and thus providing a positive replica of the plant structure. Both the plant leaves and stems were zeolitized and the calcined stems replicas showed better mechanical stability compared to the leaves replicas. The replicas contained hierarchical pores, micro−meso (leave replica) or micro−macro (stem replica). SEM images at two different magnifications of a replica of the plant leave are shown in Figure 8.

Other Macrotemplates and Methods Used To Prepare Hierarchical Zeolites. Macroporous anion-exchange resin beads have been used as macrotemplates for the synthesis of mesoporous zeolite spheres employing synthesis solutions yielding colloidal zeolites.[151,152] Macroporous anion-exchange resins are commercially available in a variety of bead sizes; they have a permanent pore structure to allow zeolite crystallization within the resin structure, are able to exchange the anions which are present in the zeolite synthesis solutions, and can easily be removed after the synthesis by calcination. The final zeolite spheres obtained were solid with a size and shape similar to that of the initial resin beads and mesoporosity emanating from the resin removal (Figure 9). Actually, this is the only example of a procedure allowing the synthesis of solid spheres by macrotemplating. In addition, the resin-zeolite composite beads showed residual ion-exchange capacity, which was used to introduce various metal anions prior to calcination and thus extraframework metal oxides evenly distributed throughout the zeolite spheres were prepared.[153,154]

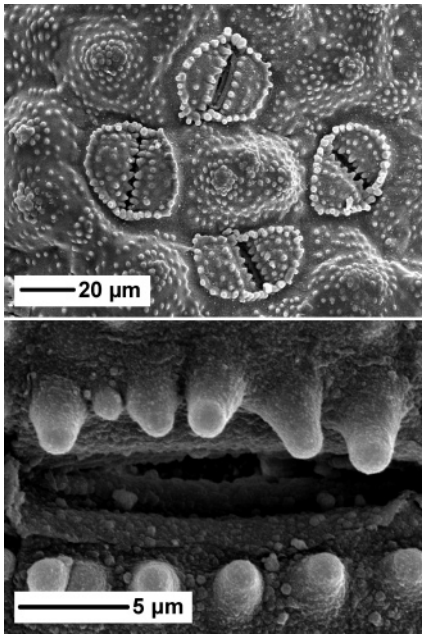

Figure 8. SEM micrographs at two different magnifications of silicalite-1 replica of an *Equisetum arvense* leaf, where stomata structures can be seen.

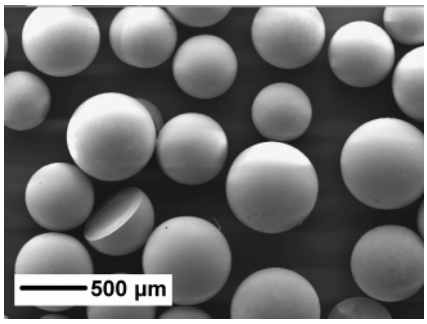

Figure 9. Electron micrograph of solid zeolite spheres prepared by resin templating.

Other organic macrotemplates have been used to prepare structured zeolites. Cellulose acetate filter membrane has been employed for the fabrication of self-supporting porous zeolite membranes with spongelike architectures and zeolitic microtubes.[155] The template membrane was electrostatically seeded with silicalite-1 crystals and the mechanical strength of the product was improved by secondary vapor-phase treatment or hydrothermal treatment in a synthesis mixture. Spongelike macroporous silicalite-1 monoliths have been obtained by starch gel templating.[156] Two methods were used, namely, incorporation of 50 nm sized zeolite nanoparticles into starch gels followed by drying and calcination, and infiltration of colloidal suspensions of zeolite nanoparticles into frozen and thawed starch gels. Hierarchical zeolite structures with designed shapes have been prepared by gel-casting of colloidal nanocrystal suspensions.[157] Thus, silicalite-1 crystal suspensions were mixed with organic monomers and casted into molds, where the monomers polymerized to yield a mechanically strong solidified suspension, which could easily be removed from the mold and sintered to obtain the final shaped monolith.

Self-standing and optically transparent silicalite-1 membranes with well-defined shapes and controlled mesoporosity have been obtained by self-assembly of zeolite nanocrystals followed by high-pressure compression and secondary crystal growth via microwave treatment.[158] Zeolite nanocrystals have been used as building blocks for the preparation of micropatterned films, micro-macroporous materials, self-standing membranes, and long zeolite fibers.[159]

3.2. Organically Functionalized Zeolite Nanocrystals and Their Uses. The zeolite applications are mainly related to the huge regular intracrystalline space. However, the large external surface area of nanosized particles also offers attractive possibilities. For instance, the rich surface chemistry of molecular sieve crystals can be used for immobilization of enzymes, which are among the most active and selective catalysts for many chemical reactions of industrial interest. The immobilization of an enzyme on an appropriated surface would increase its stability and in some cases improve the reactivity and selectivity. Different carriers such as organic resins, silica particles, and MCM-41 type mesoporous materials have been already used for immobilization of enzymes via electrostatic bonding. The advantage that might offer the external zeolite surface with respect to these materials is the regular distribution of surface silanols which allows a uniform grafting. Recently, nanosized entities obtained by delamination of zeolite ITQ-6 were employed as a carrier for β-galactosidase from *Aspergillus oryzae* and for penicillin G actylase from *Escherichia coli*.[160] This study demonstrated the possibility for covalent grafting of the enzymes on the zeolite surface. The potential of enzymes/nanozeolite composites was proven by the higher stability with respect to free enzymes and those immobilized on amorphous silica.

Another example for using the external surface of zeolite nanocrystals is the very recently published isolation and identification of phosphopeptides by metal-ion-immobilized zeolite Beta nanoparticles.[161] The phosphorylation of proteins is an important issue since it is a powerful tool to regulate almost all aspects of cell life in both prokaryotes and eukaryotes. Thus, the developed identification technique based on the Fe^{3+}-modified zeolite nanoparticles opens up new possibilities for isolation of phosphopeptides.

The external surface of zeolite nanoparticles (BEA-type) was also used for covalent grafting of two phosphonic acids with the semicarbazide group.[162] The semicarbazide functionality is known for its high reactivity with aldehydes and derivatives in mild conditions and thus the hybrid materials nanoparticles can be used in different areas of life science.

3.3. Employment of Preformed Nanocrystals for the Tailored Synthesis of Porous Solids. *3.3.1. Application of Nanozeolites as Seeds for Zeolite Syntheses.* It is well-known that seeding a molecular sieve synthesis mixture frequently has beneficial effects, for example, in controlling the particle size of the product, avoiding the need for an organic template, accelerating the synthesis, and improving the proportion of product of the intended structure type. The discrete nature of zeolite nanoparticles and their homogeneous distribution in the colloid make them very convenient for seeding zeolite synthesis gels. Colloidal zeolite seeds have already proven to be especially effective in the zeolite industrial production.[163−168] Such nanocrystals can also be employed in very specific syntheses like, for instance, the incorporation of Ti in the BEA-type framework[169] or synthesis of nanosized ZSM-5 crystals.[170]

3.3.2. Micro-/Mesoporous Materials Prepared by Utilization of Zeolite Nanocrystals or Their Precursors. To fully exploit the potential of mesoporous molecular sieves in the area of catalysis, a substantial improvement in their acidity and hydrothermal stability is required. One of the approaches that have gained much attention in recent years is the surfactant-assisted assembly of subcolloidal zeolite precursors. The procedure includes two stages. During the first stage, a zeolite precursor system is prepared and subjected to aging at room or elevated temperature to promote the formation of zeolite nanocluster precursors. During the second stage these precursors are integrated in the walls of a structured mesoporous material. Thus, different mesoporous materials using zeolite Y,[171] ZSM-5,[172] zeolite Beta,[172] TS-1,[173] and silicalite-1[174,175] precursors were synthesized. Indeed, these materials showed improved hydrothermal stability compared to their analogues synthesized by the traditional synthesis approach. The improved properties were attributed to the zeolite connectivity in the mesoporous network. Some later findings, however, point to the specific role of heteroatoms, namely, aluminum, usually present in the proto-zeolite entities. Thus, according to the study of Han et al.,[176] the crucial factors for the enhanced hydrothermal stability are the heteroatoms (Al or Ti) which (i) block the terminal OH^- groups and protect the mesoporous framework from the attack of water molecules and (ii) repel the access of OH^- ions that catalyze the hydrolysis of the framework.

The use of nanozeolite catalysts could reduce the mass transport limitations since the diffusion path is relatively short and the accessibility of the catalytic sites through the external surface is high. On the other hand, nanosized zeolites cannot be used directly due to the much higher pressure drops in packed-bed reactors. Therefore, micro-/mesoporous composites containing well-defined zeolite nanocrystals are of interest for reactions where bulky molecules are processed. Different approaches have been developed to prepare composites of uniformly distributed zeolite nanocrystals in a mesoporous matrix. The preparation procedures vary from partial re-crystallization of mesoporous walls[177−179] to mechanical mixing of zeolite nanocrystals and structured mesoporous materials.[180] Dual templating syntheses were employed by several research groups for the synthesis of micro-/mesoporous composites.[181−184] Short time hydrothermal treatment of precursor solutions resulting in non fully crystalline zeolite Beta nanocrystals was used for the synthesis of micro-/mesoporous materials by addition of a surfactant agent[185] or an initial solution yielding a mesophase[186] followed by hydrothermal treatment at elevated temperatures. On and Kaliaguine have obtained a bimodal porous material by the formation of the amorphous mesoporous precursor followed by the crystallization of the amorphous walls with the zeolitic precursor.[187,188] A simple and effective method for controlled incorporation of various

types of zeolite nanocrystals in a three-dimensional TUD-1 type mesoporous matrix was developed very recently.[189]

The catalytic performance of these composites is a matter of discussion since fairly different data were published. For instance, Maschmeyer and co-workers showed that zeolite Beta nanocrystals included in the mesoporous matrix possess higher cracking activity per gram zeolite of pure nanosized zeolite Beta for the model feed *n*-hexane.[189] On the other hand, Liu et al. did not find any substantial difference, before steaming, between Al−MCM-41 synthesized by a conventional method and by using a zeolite precursor system.[171] In another case, a positive effect on the catalytic performance was observed by simple mechanical mixing of micro- and mesoporous components.[180] Thus, the synergism between micro- and mesoporous phases included in the composite body is still not well-established. This is, however, a promising route that might bring a dual catalytic functionality and decrease the pressure drop in the reactor.

3.4. Emerging Applications of Zeolite Nanocrystals. Microporous zeolite-type materials are usually fabricated in the form of micronsized particles and further processing is needed to be employed in different areas of process industries. For this purpose, they need to be shaped, together with a binder matrix, into bodies of suitable size, geometry, and mechanical strength.[103] The distribution of zeolite particles and pore texture of these bodies should be such that the properties of the embedded crystals are not negatively affected. However, a relatively high degree of aggregation is typical of micrometer-sized zeolite products, and upon spray drying, extrusion, or drop coagulation, further aggregation of zeolite particles usually takes place. The nanosized zeolites prepared in the form of stable colloidal suspensions offer the advantage of a homogeneous initial precursor which can be uniformly distributed in a matrix. It was shown that 10−20 nm zeolite crystallites can be uniformly distributed in an alumina matrix with predefined pores driven by the opposite surface charges.[190,191] Therefore, in the traditional areas of zeolite applications such as heterogeneous catalysis, molecules separation, and ion exchange, the nanosized zeolites could bring better performance of the material due to the uniformity of distribution and accessibility of the active phase. The nanosized zeolites are also preferred in all processes where a higher reaction rate is required. Besides the impact on the traditional areas of applications, the availability of zeolite nanocrystals in the form of stable colloidal suspensions opens new possibilities for processing these materials (see section 3.1) and respectively to extend the application of microporous material to new areas which will be reviewed in this section.

Prior to any kind of application, the organic structure-directing agent (SDA) used for the synthesis of a microporous material has to be removed to take advantage of the zeolite microporosity. However, the most commonly used high-temperature combustion of the SDA provokes significant irreversible aggregation between zeolite nanoparticles due to the formation of Si−O−Si bridges. Thus, procedures that allow the liberation of zeolite microporosity with a minimum degree of aggregation are highly required. At present, three methods for template removal that allow redispersion of zeolite nanoparticles and preparation of colloidal suspensions of template-free nanoparticles have been reported. Yan and co-workers have used an organic polymer network as a temporary barrier to avoid nanocrystal aggregation during the combustion of the SDA.[192] The second procedure includes surface grafting of colloidal zeolite particles by an aminoethylphosphonic acid or an (aminopropyl)triethoxysilane that prevent the aggregation during subsequent calcination.[193] Acid extraction of the SDA from surface-functionalized zeolite nanoparticles is the third reported approach.[194] In this case the organic ligands grafted to the surface of zeolite nanoparticles have a dual function, as functionalizing and protective groups against framework alteration during the template extraction. This is an interesting approach which avoids the high-temperature calcination; however, the employed mild-solvent extraction cannot completely remove the SDA.

3.4.1. Nanozeolite-Based Sensing Materials. Microporous zeolite-type materials possess a number of physicochemical properties that make them attractive for chemical sensing, zeolite-modified electrodes (ZME), host−guest systems, etc. For instance, the uniform pores of microporous materials can display molecular recognition, discrimination, and organization properties with a resolution of less than 1 Å. Their hydrophilic/hydrophobic properties can be finely tuned by changing the framework composition and synthesis conditions. Finally, thermal, chemical, and attrition stability of the zeolites allow utilizations under severe conditions. All these characteristics make the zeolites perfect materials for sensing applications. However, there are drawbacks in the utilization of micrometer-sized zeolite crystals for advanced devices. First, the requirements for uniformity and spatial arrangements are difficult to achieve with the employment of large crystals. Second, the reaction kinetics and response time are slower for large crystals and thus it is desirable to reduce their size to achieve a faster transport and equilibration. Thus, the zeolite nanocrystals and integrated films prepared from such nanocrystals are indispensable for the preparation of new generation sensing devices. The feasibility of such devices was demonstrated by LTA-,[195] BEA-,[196] and MFI-type[119] films on quartz crystal microbalances (QCMs). Zeolite A modified sensors showed a remarkable selectivity at low water vapor concentrations and short response time. In comparison with LTA-type, the BEA-type zeolite sensors showed a higher sorption capacity for different hydrocarbons (pentane, hexane, and cyclohexane), although no selectivity was observed. High sensitivity toward organic molecules was demonstrated by the highly hydrophobic all-silica analogue with MFI-type framework.

Another possible sensing application of nanosized zeolites was reported recently. It concerns attenuated total reflection (ATR) and internal reflection (IR) elements that proved to be one of the most promising sensing materials within the modern analytical chemistry. A silicon internal reflection element was coated with a silicalite-1 film using nanosized seeds and tested in the detection of organic molecules in a gas flow.[197] The promising results suggest that new applications in FTIR-ATR spectroscopy of zeolite-modified ATR elements can be envisaged.

The preparation of a uniform, defect-free zeolite films on conductive electrodes could not be achieved without the utilization of nanosized zeolite crystals. Recently, three examples of ZME prepared by secondary growth of nanosized zeolite seeds have been reported. Kornic and Baker synthesized oriented zeolite A films which can be modified to reject or pass molecular oxygen to the underlying SnO_2 electrode.[198] The layer-by-layer (LbL) technique and secondary growth were employed for the preparation of FAU-type zeolite modified Pt and glass carbon electrodes.[199] The accumulation ability and selectivity of these materials were tested in metal ions (Ag^+, Cd^{2+}, and Pb^{2+}) recognition. Thus, the LbL-prepared electrodes showed short concentration and response time, while those prepared by secondary growth exhibited high accumulation ability. A FAU-type zeolite film was also grown on glassy carbon embedded in a resin matrix.[200] The nanosized organic template-free seeds were synthesized at room temperature, whereas the zeolite film was grown under low-temperature conditions (40 °C) to minimize the effect of the hydrothermal treatment on the electrode properties. The resultant electrodes tested in model electroactive probes or analytes ($Ru(NH_3)_6^{3+}$, $Fe(CH)_6^{3-}$, $Ru(bpy)_3^{2+}$, dopamine, ascorbic acid) showed an advantageous combination of electrochemical detection with charge and size selectivity.

FAU-type zeolite is one of the preferred hosts with its large super cage (1.3 nm) able to accommodate fairly bulky molecules. Castagnola and Dutta reported the synthesis of the $Ru(bpy)_3^{2+\circ}$ complex in the cages of nano- and micrometer-sized zeolite X crystals by conventional ship-in-a bottle technique.[201] The charge separation efficiency in the nanoparticles was found to be twice as high as that of micrometer-sized crystallites, which was attributed to the increased surface-to-volume ratio of the nanocrystals.

In situ synthesis was used for the incorporation of 2-(2-hydroxyphenyl)benzothiazole (HBT) within colloidal FAU-type crystals. HBT incorporated in the zeolite nanocrystals showed a profound modification of the excited-state properties compared to solution.[202,203] This molecule is a member of a large family of molecules with excited-state intramolecular proton-transfer (ESIPT) properties, whose application may vary from UV filtering and sensing to molecular switching. Thus, such host−guest ESIPT-zeolite systems are promising candidates for time-resolved photophysical measurements and a number of other applications.

Calzaferri and co-workers have studied the incorporation of dyes in LTL-type zeolite using crystals ranging from 30 to 3000 nm and used them for optical antenna systems.[204,205] The optical antenna systems showed light harvesting and transport properties that can be used to realize a device in which different dye molecules inside zeolite channels are arranged in such a way that the whole visible spectrum can be used by conducting light from blue to green to red without significant loss. Such materials are of interest for the preparation of a dye laser of extremely small size, as probes in near field microscopy and as materials for new imaging techniques as luminescent probes in biological systems.

3.4.2. Low-k Zeolite Films. Over the past few decades, the speed of integrated circuits has been increased by packing in more transistors that are smaller and faster. This, however, causes a resistance-capacitance delay, which is expected to become a serious limitation to performance improvement. A way to bring down capacitance is to use materials with lower dielectric constant than conventional SiO_2. Low *k*-materials are used as thin films of ca. 500 nm. Currently, there are two methods for film deposition, spin-coating, and chemical vapor deposition. Generally, the dielectric constant *k* can be decreased by decreasing the density of the materials. Porosity can be introduced into low *k*-films during film deposition through the way of packing of the primary particles or by the addition of, e.g., thermally degradable substances (porogens), upon removal of which pores are left behind. There are many challenges for the development of alternative low-*k* materials: the films should be thin and uniform, mechanically, thermally, chemically, and physically stable, hydrophobic (water has a *k* value close to 80 and small amounts of adsorbed water significantly increase the total *k* value), heat-conductive, and compatible with other materials.

Recently, pure silica zeolites were suggested as alternative candidates for the preparation of low-*k* films. They are porous, thermally stable, and hydrophobic in nature with good thermal conductivity. Thin (250−500 nm) silicalite-1 films have been prepared by in situ crystallization or by spin-coating of uniform 50 nm nanocrystals followed by a brief secondary growth using microwave radiation to improve the mechanical stability of the spin-on films.[206] The films prepared were mechanically polished to obtain smooth surfaces. The dielectric constant of the in situ crystallized as-synthesized and calcined films was 3.4 and 2.7, respectively. The *k* value of the calcined film increased to 3.3 upon exposure to air at 60% humidity. The dielectric constant of calcined spin-on films was in the range 1.8−2.1; however, the films suffered from low mechanical stability. After secondary growth, the calcined film exhibited a *k* value of 3.0. The spin-on procedure has been improved and ultralow-*k* silicalite-1 films have been prepared by using a zeolite nanoparticle suspension with an amorphous silica component as spin-on solution without the necessity to improve the mechanical stability of the films.[207] The corresponding calcined films showed a *k* value of 2.3, which increased to 3.9 upon exposure to air with 60% humidity. The films were further silylated to increase the hydrophobicity and a *k* value of 2.1 was measured with only a slight increase with exposure time. Later, the same group reported the preparation of ultralow-*k* silicalite-1 films using the spin-on procedure and addition of 5−15 wt % porogen (γ-cyclodextrin).[208] The *k* value of the films decreased from 2.3 to 1.8 for the porogen-free and the 15 wt % γ-cyclodextrin-containing films, respectively, while maintaining good mechanical stability. Another method to decrease the *k* value of the spin-on films has been reported by the same group.[209] It was found that employing colloidal suspensions of higher crystallinity led to films with lower *k*, e.g., 1.6 for a silylated film, and lower moisture sensitivity, 1.8, after exposure to ambient conditions for 24 h.

The use of the spin-coating procedure for the preparation of thin silicalite-1 films has been independently reported by

Mintova and Bein.[210] They used ethanol suspensions of 30 and 60 nm sized zeolite particles and obtained very homogeneous zeolite films. The thickness of the films could be controlled by the concentration of the zeolite suspension or by the number of spin-coating depositions. It was found that the type of the substrates did not influence the quality of the films, whereas the size of the zeolite nanocrystals influenced the preferred orientation of the films. Silicalite-1 films with thicknesses 290−400 nm have been prepared by spin-coating from purified 60 and 120 nm and as-prepared 200 nm silicalite-1 suspensions in ethanol and corresponding *k* values (calcined films) of 2.2, 2.56, and 2.1 have been determined.[211] The dielectric constant of those films decreased to 2 by depositing a spin-on acryl latex layer onto the silicalite-1 films. The role of the polymer film was to decrease the surface roughness and hydrophilicity and to increase the mechanical stability of the dielectric material.

Pure-silica zeolite Beta films, another candidate for low-*k* materials, have been prepared by spin-coating from a 100 nm zeolite Beta colloidal suspension in ethanol.[35] Although without using colloidal suspensions, the preparation of thick (15 μm) pure-silica zeolite Beta films is mentioned here to illustrate the potential of this type of films as low-*k* materials.[212] The films were in situ crystallized from a gel in fluoride media and corresponding as-synthesized films showed a dielectric constant of 2.3.

3.4.3. Nanozeolite and Medical Diagnostics. A new area where the nanozeolites could be used is medical diagnostics, in particular, magnetic resonance imaging (MRI). A recent study revealed the potential of Gd^{3+}-loaded NaY nanoparticles,[213] which have a relaxivity that is substantially higher than that of micrometer-sized zeolite crystals.[214] The results of this study demonstrate that the Gd^{3+} ion is immobilized in the interior of the zeolite and that the relaxivity is mainly limited by the relatively slow diffusion of water protons from the pores of the zeolite channels into the bulk water. Based on the findings of this study, the authors suggest the key features that have to be taken into account to design new porous materials that display high relaxivity for application as contrast agents in MRI. They are as follows: (i) the material should be able to retain Gd^{3+} ions inside the framework with as many inner-sphere water molecules as possible; (ii) the Gd^{3+} ions must be strongly coordinated to the framework to ensure a long rotational correlation time; and (iii) the pores should be big enough to allow water molecules to diffuse from the interior of the material to the bulk water. Thus, zeolite nanoparticles with large pore channel systems are expected to allow a more efficient water exchange rate.

3.4.4. Separation Materials. New high-performance materials are required not only for emerging technologies but also in all industrial fields including areas with a long history like the separation of hydrocarbons. For example, the enhancement of the octane number by separation of double-branched paraffins from single-branched and normal paraffins is of great industrial interest. However, the separation by distillation or by equilibrium-induced adsorption processes is not economically interesting for organic molecules with close thermodynamic properties. Thus, a specially designed material able to separate and store single-branched paraffins from highly branched ones is highly required. Very recently, such a material was realized in the form of a core−shell structure, where the high adsorption capacity material is the core and the shell is a zeolite with high separating power.[215] The synthesis of such a reactor was exemplified by combining all-silica analogues with BEA-type (framework density 15.1 T/1000 Å^3) and MFI-type (framework density 17.9 T/1000 Å^3) framework topologies. The overgrowth of the large core crystals was achieved by a preseeding of the support and secondary growth of deposited nanoseeds. A SEM micrograph of the core−shell zeolite Beta-silicalite-1 microcomposite is shown in Figure 10. Adsorption tests showed a high integrity of the shell layer, which covers 86% of core crystals after a single-step synthesis and 99% after a triple-step synthesis.

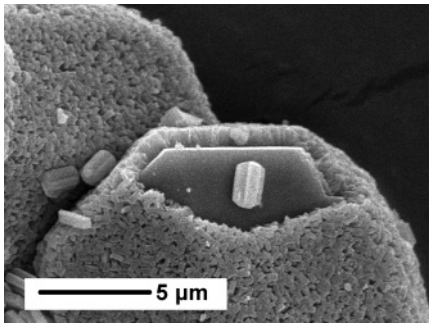

Figure 10. Electron micrograph of a core−shell Beta-silicalite-1 composite, where the uniform layer of silicalite-1 overgrown on a large zeolite Beta crystal can be seen.

Concluding Remarks

Although the first examples of syntheses of colloidal zeolite particles can be found in the early 1970s,[103,216] almost 20 years was needed for these materials to attract the interest of academic and applied scientists. The great interest in the nanosized microporous materials at the beginning of the new millennium is a part of the revolution in nanotechnology, which is expected to make most products lighter, stronger, cleaner, less expensive, and more precise. The significance of these materials for modern technology is exemplified by the burst of scientific publications devoted to nanozeolites. For the past 3 years, the number of publications has tripled with respect to the previous decade. We believe that this is the beginning of a long-lasting and fruitful period in zeolite nanotechnology, having in mind the diversity of possible areas of application, which are far beyond the traditional catalytic, ion-exchange, and adsorption uses. The objective of the present review was to summarize the trends in the synthesis, processing, and potential areas of application of nanosized zeolite crystals.

Among the different approaches developed for the synthesis of zeolite nanocrystals, the utilization of initially clear solutions is the most effective and widely used. The solid products of such syntheses are in the form of stable colloidal suspensions with relatively narrow particle size distributions. The discrete particles are very often single crystals, which make these systems very convenient for the investigation of crystal nucleation and growth. The most important materials

from a practical viewpoint, for instance, the MFI-, BEA-, FAU-, and LTA-type solids, have been prepared using this synthetic approach. On the other hand, the synthesis of nanosized zeolite crystals from initially clear solutions is far from being optimized. For instance, the reproducibility of the syntheses, except for silicalite-1, is not very high. The yields are also relatively low, mainly due to the low crystallization temperatures usually used. Another concern is the high amount of tetraalkylammonium hydroxides used which cause both environmental and economical problems. Probably, a substantial part of these problems could find a solution, for instance, with use of seeds and reuse of nonreacted reagents. This synthetic route is, however, not universal and cannot be employed for all types of microporous materials. Lately, a number of fascinating new microporous materials were synthesized by using the fluoride route, where dense hydrogels and close to neutral synthesis media were employed.[217−221] Such conditions, i.e., low supersaturation and high aggregation of the initial particles, are favorable for the synthesis of large micrometer-sized crystals. In addition, the crystallization field of these new microporous materials is relatively narrow and changes in the gel formulation could lead to formation of other solids. Thus, the synthesis of zeolite nanocrystals of microporous materials that crystallize at low supersaturation is a challenge that remains to be met. Scaling up the synthesis and postsynthesis processing of colloidal zeolites is another issue that should be resolved. On a laboratory scale, two methods of purification of colloidal zeolite particles from nonreacted organic and inorganic species are used at present. The first comprises a series of high-speed centrifugation and redispersion in water, while the second is based on the utilization of dialysis medical devices. Both approaches are not applicable on a large scale, which suggests that for the industrial-scale purification of colloidal zeolites a specific engineering solution has to be found. Also the removal of the organic template from zeolite nanoparticles with minimum aggregation so as to keep their colloidal nature does not seem to be an easy task.

Even though a rational control of the synthesis of colloidal zeolites is still not achieved, the systems yielding colloidal zeolites bring new insights into the zeolite nucleation/crystallization mechanism. Thus, the formation of LTA-type zeolite nanocrystals at room temperature allowed visualizing the "birth" of the zeolite. The emerging of a crystalline structure at the center of each gel particle and its propagation through the gel network until complete transformation into a zeolite was recorded by means of high-resolution transmission electron microscopy. On the other hand, a study of a system yielding FAU-type nanocrystals at room temperature revealed that the crystallization stages of the zeolite can be dominated by a different crystallization mechanism. A crystal growth by propagation through the gel phase dominated during the first period (10−15 wt % transformation into a zeolite), while the crystallization process was governed by spontaneous aggregation and crystallization of nanoparticles around a crystallization center. The formation of silicalite-1 from clear solutions was a subject of numerous in and ex situ investigations performed with a large set of complementary techniques. It is now accepted that formation of silicalite-1 occurs via the formation of 2−4 nm colloidal entities, which according to some authors possess the characteristic features of the MFI-type framework topology. The utilization of nanozeolite-yielding precursor systems was of great importance for collecting all these new findings, which complement the information based on the investigation of conventional zeolite precursor systems. Obviously, the nanozeolite precursor systems are very convenient for fundamental studies of the zeolite nucleation/crystallization mechanisms and will be widely used in future studies.

Considering the publication activity in the field, it seems that the focus of the scientific community has moved from the synthesis to the potential applications of nanosize microporous materials. In contrast to the publications in the 1990s, devoted exclusively to the synthesis of zeolite nanocrystals, in the past several years the main part of publications concerned the utilization of zeolite colloids. This is related to the fascinating opportunities offered by the crystal size decreased to several unit cells. The impact of the crystal size reduction on kinetics of reaction and transport via microporous media could bring higher efficiency in certain catalytic and separation processes. Decreasing the crystal size is probably the simplest way to overcome the mass transport limitations and ensure high accessibility of the catalytic sites. On the other hand, the core−shell zeolite microcomposites that combine high separation power and adsorption capacity could bring new competence in separation processes. Such a configuration could be used for catalytic microreactors containing cores and shells with different catalytic abilities.[222] Further, the possibility to use well-defined nanocrystallites with narrow particle size distributions will bring new opportunities in chemical sensing and electrochemical analysis. For instance, the desire of the electrochemists to achieve an intelligent design of the surface of conventional electrodes could become a reality by means of microporous nanocrystals. The new functionality that could be brought by the zeolite nanocrystals is mainly related to the possibility to grow very thin (100−200 nm) defect-free zeolite films with close contact to the detecting device. In this way, devices combining fast transport with outstanding size and chemical selectivity could be designed. Optical antennas, dye lasers of extremely small size, probes for near field microscopy, or new imaging luminescent probes are only a few of the possible future applications of functionalized zeolite nanocrystals. All-silica microporous materials are among the major candidates that could fulfill the requirements of the future generation of microprocessors, where dielectric materials with k below 2.2 will be needed. A new field where the zeolite nanocrystals have made the first encouraging steps is medical diagnostics. Contrast and luminescent agents were successfully introduced into zeolite nanocrystals and their external surface was functionalized by molecules that can be used for genes grafting. Thus, it is not difficult to envisage the preparation of nanozeolite-based "integrated chemical systems", where the intracrystalline volume is charged with a contrast agent or a luminescent material while the large external surface of nanocrystallites is functionalized in a way to bring the probe to the desired

target. It is worth recalling also the preparation of microcapsules built of intergrown zeolite shells. The possibility to encapsulate and controllably release active ingredients will certainly be very useful for pharmaceutical and cosmetic applications.

This listing of potential applications of zeolite nanocrystal is not exhaustive. Nevertheless, it gives an idea about the diversity of possible uses of nanozeolites, which range from medicine to electronics. To this large variety of new promising applications, one has to add the impact of nanozeolites on traditional application areas of zeolites. Last, but not least, the evolution of zeolite precursor systems is a convenient tool bringing new insights into the mechanism of zeolite formation. Hence, it is not very risky to predict a growing interest and new, fascinating developments in the area of nanosized microporous materials.

Acknowledgment. The authors thank the CNRS-DFG bilateral program for financial support.

Abbreviations

DLS = dynamic light scattering
SAXS = small-angle X-ray scattering
USAXS = ultra small-angle X-ray scattering
SANS = small angle neutron scattering
WAXS = wide-angle X-ray scattering
IR = infrared
DSC = differential scanning calorimetry
SEM = scanning electron microscopy
TEM = transmission electron microscopy
AFM = atomic force microscopy
GPC = gel permeation chromatography
XRS = X-ray scattering
UV−Vis = ultraviolet visible spectroscopy
EDX = energy-dispersive X-ray

References

(1) Cundy, C. S.; Cox, P. A. *Chem. Rev.* **2003**, *103*, 663.
(2) Stein, A. *Adv. Mater.* **2003**, *15*, 763.
(3) Schüth, F.; Schmidt, W. *Adv. Mater.* **2002**, *14*, 629.
(4) Davis, M. E. *Nature* **2002**, *417*, 813.
(5) Feoktistova, N. N.; Zhdanov, S. P.; Lutz, W.; Bülov, M. *Zeolites* **1989**, *9*, 135.
(6) Mintova, S.; Valtchev, V. *Zeolites* **1993**, *3*, 136.
(7) Valtchev, V. P.; Bein, T. Patent No. WO0240403, 2003.
(8) Zhan, B.-Z.; White, M. A.; Lumsden, M.; Mueller-Neuhaus, J.; Robertson, K. N.; Cameron, T. S.; Gharghouri, M. *Chem. Mater.* **2002**, *14*, 3636.
(9) Schoeman, B. J.; Sterte, J.; Otterstedt, J.-E. *Zeolites* **1994**, *14*, 110.
(10) Mintova, S.; Valtchev, V. *Stud. Surf. Sci. Catal.* **1999**, *125*, 141.
(11) Mintova, S.; Olson, N. H.; Bein, T. *Angew. Chem., Int. Ed.* **1999**, *38*, 3201.
(12) Zhu, G.; Qiu, S.; Yu, J.; Sakamoto, Y.; Xiao, F.; Xu, R.; Terasaki, O. *Chem. Mater.* **1998**, *10*, 1483.
(13) Valtchev, V. P.; Bozhilov, K. N. *J. Phys. Chem. B* **2004**, *108*, 15587.
(14) Holmberg, B. A.; Wang, H.; Norbeck, J. M.; Yan, Y. *Microporous Mesoporous Mater.* **2003**, *59*, 13.
(15) Holmberg, B. A.; Wang, H.; Yan, Y. *Microporous Mesoporous Mater.* **2004**, *74*, 189.
(16) Li, Q.; Creaser, D.; Sterte, J. *Chem. Mater.* **2002**, *14*, 1319.
(17) Li, Q.; Creaser, D.; Sterte, J. *Stud. Surf. Sci. Catal.* **2001**, *135*, 02−O−03.
(18) Rakoczy, R. A.; Traa, Y. *Microporous Mesoporous Mater.* **2003**, *60*, 69.
(19) Mintova, S.; Olson, N. H.; Valtchev, V.; Bein, T. *Science* **1999**, *283*, 958.
(20) Hedlund, J.; Schoeman, B.; Sterte, J. *Chem. Commun.* **1997**, 1193.
(21) Schoeman, B. J.; Sterte, J.; Otterstedt, J.-E. *Zeolites* **1994**, *14*, 208.
(22) Schoeman, B. J.; Sterte, J.; Otterstedt, J.-E. *J. Colloid Interface Sci.* **1995**, *170*, 449.
(23) Kecht, J.; Mihailova, B.; Karaghiosoff, K.; Mintova, S.; Bein, T. *Langmuir* **2004**, *20*, 5271.
(24) Verduijn, J. P. Patent No. WO9703019, 1997.
(25) Verduijn, J. P. Patent No. WO9703020, 1997.
(26) Hedlund, J.; Kurpan, E. *Stud. Surf. Sci. Catal.* **2001**, *135*, 224.
(27) Hincapie, B. O.; Garces, L. J.; Zhang, Q.; Sacco, A.; Suib, S. L. *Microporous Mesoporous Mater.* **2004**, *67*, 19.
(28) Meng, X.; Zhang, Y.; Meng, M.; Pang, W. In *Proceedings of the 9th International Zeolite Conference*, Montreal 1992; von Ballmoos, R., et al., Eds.; Butterworth-Heinemann: London, 1993; p 297.
(29) Tsapatsis, M.; Lovallo, M.; Okubo, T.; Davis, M. E.; Sadakata, M. *Chem. Mater.* **1995**, *7*, 1734.
(30) Anthonis, M. H.; Mertens, M. M.; Verduijn, J. P. Patent No. WO9703021, 1997.
(31) Larlus, O.; Valtchev, V. P. *Chem. Mater.* **2004**, *16*, 3381.
(32) Camblor, M. A.; Corma, A.; Mifsud, A.; Pérez-Pariente, J.; Valencia, S. *Stud. Surf. Sci. Catal.* **1997**, *105*, 341.
(33) Camblor, M. A.; Corma, A.; Valencia, S. *Microporous Mesoporous Mater.* **1998**, *25*, 59.
(34) Schoeman, B. J.; Babouchkina, E.; Mintova, S.; Valtchev, V. P.; Sterte, J. *J. Porous Mater.* **2001**, *8*, 13.
(35) Mintova, S.; Reinelt, M.; Metzger, T. H.; Senker, J.; Bein, T. *Chem. Commun.* **2003**, 326.
(36) Persson, A. E.; Schoeman, B. J.; Sterte, J.; Otterstedt, J.-E. *Zeolites* **1995**, *15*, 611.
(37) Van Grieken, R.; Sotelo, J. L.; Menéndez, J. M.; Melero, J. A. *Microporous Mesoporous Mater.* **2000**, *39*, 135.
(38) Song, W.; Justice, R. E.; Jones, C. A.; Grassian, V. H.; Larsen, S. C. *Langmuir* **2004**, *20*, 8301.
(39) Aguado, J.; Serrano, D. P.; Escola, J. M.; Rodríguez, J. M. *Microporous Mesoporous Mater.* **2004**, *75*, 41.
(40) Verduijn, J. P. Patent No. WO9308125, 1993.
(41) Persson, A. E.; Schoeman, B. J.; Sterte, J.; Otterstedt, J.-E. *Zeolites* **1994**, *14*, 557.
(42) Schoeman, B. J.; Sterte, J. *KONA* **1997**, *15*, 150.
(43) Tsay, C. S.; Chiang, A. S. T. *Microporous Mesoporous Mater.* **1998**, *26*, 89.
(44) Li, Q.; Creaser, D.; Sterte, J. *Microporous Mesoporous Mater.* **1999**, *31*, 141.
(45) Yang, S.; Navrotsky, A.; Wesolowski, D. J.; Pople, J. A. *Chem. Mater.* **2004**, *16*, 210.
(46) Song, W.; Justice, R. E.; Jones, C. A.; Grassian, V. H.; Larsen, S. C. *Langmuir* **2004**, *20*, 4696.
(47) Valtchev, V. P.; Faust, A.-C.; Lézervant, J. *Microporous Mesoporous Mater.* **2004**, *68*, 91.
(48) Li, Q.; Mihailova, B.; Creaser, D.; Sterte, J. *Microporous Mesoporous Mater.* **2000**, *40*, 53.
(49) Li, Q.; Mihailova, B.; Creaser, D.; Sterte, J. *Microporous Mesoporous Mater.* **2001**, *43*, 51.
(50) Mintova, S.; Petkov, N.; Karaghiosoff, K.; Bein, T. *Microporous Mesoporous Mater.* **2001**, *50*, 121.
(51) Dong, J.-P.; Zou, J.; Long, Y.-C. *Microporous Mesoporous Mater.* **2003**, *57*, 9.
(52) Zhang, G.; Sterte, J.; Schoeman, B. J. *Chem. Mater.* **1997**, *9*, 210.
(53) Cundy, C. S.; Forrest, J. O.; Plaisted, R. J. *Microporous Mesoporous Mater.* **2003**, *66*, 143.
(54) Cundy, C. S.; Forrest, J. O. *Microporous Mesoporous Mater.* **2004**, *72*, 67.
(55) Du, H.; Fang, M.; Xu, W.; Meng, X.; Pang, W. *J. Mater. Chem.* **1997**, *7*, 551.
(56) Mintova, S.; Mo, S.; Bein, T. *Chem. Mater.* **1998**, *10*, 4030.
(57) Zhu, G.; Qiu, S.; Gao, F.; Wu, G.; Wang, R.; Li, B.; Fang, Q.; Li, Y.; Gao, B.; Xu, X.; Terasaki, O. *Microporous Mesoporous Mater.* **2001**, *50*, 129.
(58) Vilaseca, M.; Mintova, S.; Karaghiosoff, K.; Metzger, T. H.; Bein, T. *Appl. Surf. Sci.* **2004**, *226*, 1.
(59) Hosokawa, H.; Oki, K. *Chem. Lett.* **2003**, *32*, 586.
(60) Mintova, S.; Valtchev, V. *Microporous Mesoporous Mater.* **2002**, *55*, 171.
(61) Cundy, C. S.; Forrest, J. O.; Plaisted, R. J. *Stud. Surf. Sci. Catal.* **2000**, *135*, 02-O-02.
(62) Cundy, C. S.; Forrest, R. J. *Stud. Surf. Sci. Catal.* **2000**, *135*, 02-P-08.
(63) Madsen, C.; Jacobsen, C. J. H. *Chem. Commun.* **1999**, 673.
(64) Schmidt, I.; Madsen, C.; Jacobsen, C. J. H. *Inorg. Chem.* **2000**, *39*, 2279.
(65) Jacobsen, C. J. H.; Madsen, C.; Janssens, T. V. W.; Jakobsen, H. J.; Skibsted, J. *Microporous Mesoporous Mater.* **2000**, *39*, 393.
(66) Kim, S.-S.; Shah, J.; Pinnavaia, T. J. *Chem. Mater.* **2003**, *15*, 1664.
(67) Naik, S. P.; Chen, J. C.; Chiang, A. S. T. *Microporous Mesoporous Mater.* **2002**, *54*, 293.
(68) Naik, S. P.; Chiang, A. S. T.; Thompson, R. W.; Huang, F. C. *Chem. Mater.* **2003**, *15*, 787.
(69) Pham-Huu, C.; Winé, G.; Tessonnier, J.-P.; Ledoux, M.-J.; Rigolet, S.; Marichal, C. *Carbon* **2004**, *42*, 1946.
(70) Wang, B.; Ma, H. Z.; Shi, Q. Z. *Chin. Chem. Lett.* **2002**, *13*, 385.
(71) Wang, H.; Holmberg, B. A.; Yan, Y. *J. Am. Chem. Soc.* **2003**, *125*, 9928.
(72) Schüth, F. *Curr. Opin. Solid State Mater. Sci.* **2001**, *5*, 389.
(73) Schoeman, B. J. *Microporous Mater.* **1997**, *9*, 267.
(74) Schoeman, B. J.; Regev, O. *Zeolites* **1996**, *17*, 447−456.
(75) Schoeman, B. J. *Stud. Surf. Sci. Catal.* **1997**, *105*, 647.
(76) Watson, J. N.; Brown, A. S.; Iton, L. E.; White, J. W. *J. Chem. Soc., Faraday Trans.* **1998**, *94*, 2181.
(77) Twomey, T. A. M.; Mackay, M.; Kuipers, H. P. C. E.; Thompson, R. W. *Zeolites* **1994**, *14*, 162.
(78) Schoeman, B. J. *Zeolites* **1997**, *18*, 97.
(79) Corkery, R. W.; Ninham, B. W. *Zeolites* **1997**, *18*, 379.

(80) Watson, J. N.; Iton, L. E.; Keir, R. I.; Thomas, J. C.; Dowling, T. L.; White, J. W. *J. Phys. Chem. B* **1997**, *101*, 10094.
(81) de Moor, P.-P. E. A.; Beelen, T. P. M.; Komanschek, B. U.; Diat, O.; van Santen, R. A. *J. Phys. Chem. B* **1997**, *101*, 11077.
(82) Schoeman, B. J. *Microporous Mesoporous Mater.* **1998**, *22*, 9.
(83) De Moor, P.-P. E. A.; Beelen, T. P. M.; Komanschek, B. U.; van Santen, R. A. *Microporous Mesoporous Mater.* **1998**, *21*, 263.
(84) Ravishankar, R.; Kirschhock, C.; Schoeman, B. J.; Vanoppen, P.; Grober, P. J.; Storck, S.; Maier, W. F.; Martens, J. A.; De Schryver, F. C.; Jacobs, P. A. A. *J. Phys. Chem. B* **1998**, *102*, 2633.
(85) Ravishankar, R.; Kirschhock, C. E. A.; Schoeman, B. J.; De Vos, D.; Grober, P. J.; Jacobs, P. A.; Martens, J. A. *Proceedings 12th International Zeolite Conference*; Treacy, M. M. J., Marcus, B. K., Bisher, M. E., Higgins, J. B., Eds.; Baltimore, Maryland, 1998; Vol. III, p 1825.
(86) Ravishankar, R.; Kirschhock, C. E. A.; Knops-Gerrits, P.-P.; Feijen, E. J. P.; Grober, P. J.; Vanoppen, P.; De Schryver, F. C.; Miehe, G.; Fuess, H.; Schoeman, B. J.; Jacobs, P. A.; Martens, J. A. *J. Phys. Chem. B* **1999**, *103*, 4960.
(87) Kirschhock, C. E. A.; Ravishankar, R.; Verspeurt, F.; Grober, P. J.; Jacobs, P. A.; Martens, J. A. *J. Phys. Chem. B* **1999**, *103*, 4965.
(88) Kirschhock, C. E. A.; Ravishankar, R.; Van Looveren, L.; Jacobs, P. A.; Martens, J. A. *J. Phys. Chem. B* **1999**, *103*, 4972.
(89) Kirschhock, C. E. A.; Ravishankar, R.; Jacobs, P. A.; Martens, J. A. *J. Phys. Chem. B* **1999**, *103*, 11021.
(90) Kirschhock, C. E. A.; Ravishankar, R.; Truyens, K.; Verspeurt, F.; Grober, P. J.; Jacobs, P. A.; Martens, J. A. *Stud. Surf. Sci. Catal.* **2000**, *129*, 139.
(91) Nikolakis, V.; Kokkoli, E.; Tirrell, M.; Tsapatsis, M.; Vloachos, D. G. *Chem. Mater.* **2000**, *12*, 845.
(92) Kirschhock, C. E. A.; Buschmann, V.; Kremer, S.; Ravishankar, R.; Houssin, C. J. Y.; Mojet, B. L.; van Santen, R. A.; Grobet, P. J.; Jacobs, P. A.; Martens, J. A. *Angew. Chem., Int. Ed.* **2001**, *40*, 2637.
(93) Mintova, S.; Olson, N. H.; Senker, J.; Bein, T. *Angew. Chem., Int. Ed.* **2002**, *41*, 2558.
(94) Kirschhock, C. E. A.; Kremer, S. P. B.; Grobet, P. J.; Jacobs, P. A.; Martens, J. A. *J. Phys. Chem. B* **2002**, *106*, 4897.
(95) Yang, S.; Navrotsky, A. *Chem. Mater.* **2002**, *14*, 2803.
(96) Kragten, D. D.; Fedeyko, J. M.; Sawant, K. R.; Rimer, J. D.; Vlachos, D. G.; Lobo, R. F.; Tsapatsis, M. *J. Phys. Chem. B* **2003**, *107*, 10006.
(97) Harikrishnan, R.; Kokkoli, E.; Tsapatsis, M. *Angew. Chem., Int. Ed.* **2004**, *43*, 4558.
(98) Knight, C. T. G.; Kinrade, S. D. *J. Phys. Chem. B* **2002**, *106*, 3329.
(99) Subotic, B. *Zeolite Synthesis, ACS Symp. Ser.* **1989**, *398*, 110.
(100) Subotic, B.; Graovac, A. *Stud. Surf. Sci. Catal.* **1985**, *24*, 199.
(101) Thompson, R. W. *Zeolites* **1992**, *12*, 837.
(102) Gontier, S.; Gora, L.; Güray, I.; Thompson, R. W. *Zeolites* **1993**, *13*, 414.
(103) Breck, D. W. *Zeolite Molecular Sieves*; John Wiley&Sons: New York, 1974.
(104) Szostak, R. *Handbook of Molecular Sieves*; Van Nostrand Reinhold: New York, 1992.
(105) Barrer, R. M. *Hydrothermal Chemistry of Zeolites*; Academic Press: London, 1982.
(106) Subotic, B.; Graovac, A. *Stud. Surf. Sci. Catal.* **1985**, *24*, 199.
(107) Gora, L.; Streletzky, K.; Thompson, R. W.; Phillies, G. D. J. *Zeolites* **1997**, *18*, 119.
(108) Tschernich, R. W. *Zeolites of the World*; Geoscience Press Inc.: Phoenix, AZ, 1992.
(109) Sand, L. B.; Sacco, A.; Thompson, R. W.; Dixon, A. G. *Zeolites* **1987**, *7*, 387.
(110) Bein, T. *Chem. Mater.* **1996**, *8*, 1636.
(111) Tavolaro, A.; Drioli, E. *Adv. Mater.* **1999**, *11*, 975.
(112) Caro, J.; Noack, M.; Kölsch, P.; Schäfer, R. *Microporous Mesoporous Mater.* **2000**, *38*, 3.
(113) Chiang, A. S. T.; Chao, K. *J. Phys. Chem. Solids* **2001**, *62*, 1899.
(114) Noack, M.; Kölsch, P.; Schäfer, R.; Toussaint, P.; Caro, J. *Chem. Eng. Technol.* **2002**, *25*, 221.
(115) Coronas, J.; Santamaria, J. *Top. Catal.* **2004**, *29*, 29.
(116) Nair, S.; Tsapatsis, M. *Handbook of Zeolite Science and Technology*; Auerbach, S. M., Carrado, K. A., Dutta, P. K., Eds.; Marcel Dekker: New York, 2003; p 869.
(117) Lovallo, M. C.; Boudreau, L.; Tsapatsis, M. *Mater. Res. Soc. Symp. Proc.* **1996**, *431*, 225.
(118) Hedlund, J.; Schoeman, B. J.; Sterte, J. *Stud. Surf. Sci. Catal.* **1997**, *105*, 2203.
(119) Mintova, S.; Schoeman, B. J.; Valtchev, V.; Sterte, J.; Mo, S.; Bein, T. *Adv. Mater.* **1997**, *9*, 585.
(120) Mintova, S.; Valtchev, V.; Engström, V.; Schoeman, B. J.; Sterte, J. *Microporous Mater.* **1997**, *11*, 149.
(121) Boudreau, L. C.; Tsapatsis, M. *Chem. Mater.* **1997**, *8*, 11705.
(122) Xomeritakis, G.; Nair, S.; Tsapatsis, M. *Microporous Mesoporous Mater.* **2000**, *38*, 61.
(123) Holmes, S. A.; Markert, C.; Plaisted, R. J.; Forrest, J. O.; Agger, J. R.; Anderson, M. W.; Cundy, C. S.; Dwyer, J. *Chem. Mater.* **1999**, *11*, 3329.
(124) Ke, C.; Yang, W. L.; Ni, Z.; Wang, Y. J.; Tang, Y.; Gu, Y.; Gao, Z. *Chem. Commun.* **2001**, 783.
(125) Shan, W.; Zhang, Y.; Yang, W.; Ke, C.; Gao, Z.; Ye, Y.; Tang, Y. *Microporous Mesoporous Mater.* **2004**, *69*, 35.
(126) Kulak, A.; Lee, Y.-J.; Park, Y. S.; Yoon, K. B. *Angew. Chem., Int. Ed.* **2000**, *39*, 950.
(127) Ha, K.; Lee, Y.-J.; Lee, H. J.; Yoon, K. B. *Adv. Mater.* **2000**, *12*, 1114.
(128) Cho, G.; Lee, J.-S.; Glatzhofer, D. T.; Fung, B. M.; Yuan, W. L.; O'Rear, E. A. *Adv. Mater.* **1999**, *11*, 497.
(129) Lai, Z.; Bonila, G.; Diaz, I.; Nery, J. G.; Sujaoti, K.; Amat, M. A.; Kokkoli, E.; Terasaki, O.; Thompson, R. W.; Tsapatsis, M.; Vlachos, D. G. *Science* **2003**, *300*, 456.
(130) Wang, X. D.; Yang, W. L.; Tang, Y.; Wang, Y. J.; Fu, S. K.; Gao, Z. *Chem. Commun.* **2000**, 2161.
(131) Valtchev, V.; Mintova, S. *Microporous Mesoporous Mater.* **2001**, *43*, 41.
(132) Holland, B. T.; Abrams, L.; Stein, A. *J. Am. Chem. Soc.* **1999**, *121*, 4308.
(133) Wang, Y. J.; Tang, Y.; Ni, Z.; Hua, W. M.; Yang, W. L.; Wang, X. D.; Tao, W. C.; Gao, Z. *Chem. Lett.* **2000**, 510.
(134) Rhodes, K. H.; Davis, S. A.; Caruso, F.; Zhang, B.; Mann, S. *Chem. Mater.* **2000**, *12*, 2832.
(135) Valtchev, V. *Chem. Mater.* **2002**, *14*, 956.
(136) Valtchev, V. *Chem. Mater.* **2002**, *14*, 4371.
(137) Valtchev, V. *J. Mater. Chem.* **2002**, *12*, 1914.
(138) Dong, A.; Wang, Y.; Tang, Y.; Zhang, Y.; Ren, N.; Gao, Z. *Adv. Mater.* **2002**, *14*, 1506.
(139) Dong, A.; Wang, Y.; Tang, Y.; Ren, N.; Zhang, Y.; Gao, Z. *Chem. Mater.* **2002**, *14*, 3217.
(140) Dong, A.; Wang, Y.; Wang, D.; Yang, W.; Zhang, Y.; Ren, N.; Gao, Z.; Tang, Y. *Microporous Mesoporous Mater.* **2003**, *64*, 69.
(141) Dong, A.; Ren, N.; Yang, W.; Wang, Y.; Zhang, Y.; Wang, D.; Hu, J.; Gao, Z.; Tang, Y. *Adv. Funct. Mater.* **2003**, *13*, 943.
(142) Song, W.; Kanthasamy, R.; Grassian, V. H.; Larsen, S. C. *Chem. Commun.* **2004**, 1920.
(143) Wang, Y.; Caruso, F. *Adv. Funct. Mater.* **2004**, *14*, 1012.
(144) Zhang, B.; Davis, S. A.; Mendelson, N. H.; Mann, S. *Chem. Commun.* **2000**, 781.
(145) Anderson, M. W.; Holmes, S. M.; Hanif, N.; Cundy, C. S. *Angew. Chem., Int. Ed.* **2000**, *39*, 2707.
(146) Wang, Y.; Tang, Y.; Dong, A.; Wang, X.; Ren, N.; Gao, Z. *J. Mater. Chem.* **2002**, *12*, 1812.
(147) Xu, F.; Wang, Y.; Wang, X.; Zhang, Y.; Tang, Y.; Yang, P. *Adv. Mater.* **2003**, *15*, 1751.
(148) Dong, A.; Wang, Y.; Tang, Y.; Ren, N.; Zhang, Y.; Yue, Y.; Gao, Z. *Adv. Mater.* **2002**, *14*, 926.
(149) Valtchev, V.; Smaihi, M.; Faust, A.-C.; Vidal, L. *Angew. Chem., Int. Ed.* **2003**, *42*, 2782.
(150) Valtchev, V. P.; Smaihi, M.; Faust, A.-C.; Vidal, L. *Chem. Mater.* **2004**, *16*, 1350.
(151) Tosheva, L.; Valtchev, V.; Sterte, J. *Microporous Mesoporous Mater.* **2000**, *35*−*36*, 621.
(152) Tosheva, L.; Mihailova, B.; Valtchev, V.; Sterte, J. *Microporous Mesoporous Mater.* **2001**, *48*, 31.
(153) Naydenov, V.; Tosheva, L.; Sterte, J. *Microporous Mesoporous Mater.* **2002**, *55*, 253.
(154) Naydenov, V.; Tosheva, L.; Sterte, J. *Chem. Mater.* **2002**, *14*, 4881.
(155) Wang, Y.; Tang, Y.; Dong, A.; Wang, X.; Ren, N.; Shan, W.; Gao, Z. *Adv. Mater.* **2002**, *14*, 994.
(156) Zhang, B.; Davis, S. A.; Mann, S. *Chem. Mater.* **2002**, *14*, 1369.
(157) Wang, H.; Huang, L.; Wang, Z.; Mitra, A.; Yan, Y. *Chem. Commun.* **2001**, 1364.
(158) Huang, L.; Wang, Z.; Wang, H.; Sun, J.; Li, Q.; Zhao, D.; Yan, Y. *Microporous Mesoporous Mater.* **2001**, *48*, 73.
(159) Huang, L.; Wang, Z.; Sun, J.; Miao, L.; Li, Q.; Yan, Y.; Zhao, D. *J. Am. Chem. Soc.* **2000**, *122*, 3530.
(160) Corma, A.; Formes, V.; Rey, F. *Adv. Mater.* **2002**, *14*, 71.
(161) Zhang, Y.; Yu, X.; Wang, X.; Shan, W.; Yang, P.; Tang, Y. *Chem. Commun.* **2004**, 2881.
(162) Doussineau, T.; Durand, J.-O.; Granier, M.; Smaihih, M.; Valtchev, V. *Synlett* **2004**, *10*, 1735.
(163) Verduijn, J. P.; Mertens, M. M.; Mortier, W. J.; Janssen, M. J. G.; Van Oorschot, C. W. M.; Vaughan, D. E. W. Patent No. WO 006492, 2000.
(164) Verduijn, J. P.; Mertens, M. M.; Mortier, W. J.; Janssen, M. J. G.; Van Oorschot, C. W. M.; Vaughan, D. E. W. Patent No. WO 006493, 2000.
(165) Verduijn, J. P.; Mertens, M. M.; Mortier, W. J.; Janssen, M. J. G.; Van Oorschot, C. W. M.; Vaughan, D. E. W. Patent No. WO 006494, 2000.
(166) Verduijn, J. P. Eur. Pat. No. 0753483, 1997.
(167) Verduijn, J. P. Eur. Pat. No. 0753484, 1997.
(168) Verduijn, J. P. Eur. Pat. No. 0753485, 1997.
(169) Blasco, T.; Camblor, M. A.; Corma, A.; Elsteve, P.; Guil, J. M.; Martinez, A.; Perdigon-Melon, J. A.; Valencia, S. *J. Phys. Chem. B* **1998**, *102*, 75.
(170) Reding, G.; Mäurer, T.; Kraushaar-Czarnetzki, B. *Microporous Mesoporous Mater.* **2003**, *57*, 83.
(171) Liu, Y.; Zhang, W.; Pinnavaia, T. J. *J. Am. Chem. Soc.* **2000**, *122*, 8791.
(172) Liu, Y.; Zhang, W.; Pinnavaia, T. J. *Angew. Chem., Int. Ed.* **2001**, *40*, 1255.
(173) Liu, Y.; Zhang, W.; Han, Y.; Xiao, F.-S. *Chem. Mater.* **2002**, *14*, 2536.
(174) Kremer, S. P. B.; Kirschhock, C. E. A.; Aerts, A.; Villani, K.; Martens, J. A.; Lebedev, O. I.; Van Tandello, G. *Adv. Mater.* **2003**, *15*, 1705.
(175) Carr, C. S.; Kaskel, S.; Shantz, D. F. *Chem. Mater.* **2004**, *16*, 3139.
(176) Han, Y.; Li, N.; Zhao, L.; Li, D.; Xu, X.; Wu, S.; Di, Y.; Li, C.; Zou, Y.; Yu, Y.; Xiao, F.-S. *J. Phys. Chem. B* **2003**, *107*, 7551.
(177) Kloetstra, K. R.; van Bekkum, H.; Jansen, J. C. *Chem. Commun.* **1997**, 2281.
(178) Huang, L. M.; Guo, W. P.; Deng, P.; Xue, Z. Y.; Li, Q. Z. *J. Phys. Chem. B* **2000**, *104*, 2817.

(179) Verhoef, M. J.; Kooyman, P. J.; van der Waal, J. C.; Rigutto, M. S.; Peters, J. A.; van Bekkum, H. *Chem. Mater.* **2001**, *13*, 683.
(180) Kinger, G.; Majda, D.; Vinek, H. *Appl. Catal. A.* **2002**, *225*, 301.
(181) Karlsson, A.; Stöcker, M.; Schmidt, R. *Microporous Mesoporous Mater.* **1999**, *27*, 181.
(182) Zhang, Z.; Han, Y.; Xiao, F.-S.; Qiu, S.; Zhu, L.; Wang, R.; Yu, Y.; Zhang, Z.; Zou, B.; Wang, Y.; Sun, H.; Zhao, D.; Wei, Y. *J. Am. Chem. Soc.* **2001**, *123*, 5014.
(183) Zhang, Z.; Han, Y.; Zhu, L.; Wang, R.; Yu, Y.; Qiu, S.; Zhao, D.; Xiao, F.-S. *Angew. Chem., Int. Ed.* **2001**, *40*, 1258.
(184) Carr, C. S.; Kaskel, S.; Schantz, D. F. *Chem. Mater.* **2004**, *16*, 3139.
(185) Guo, W.; Huang, L.; Deng, P.; Xue, Z.; Li, Q. *Microporous Mesoporous Mater.* **2001**, *44*−*45*, 427.
(186) Prokesova, P.; Mintova, S.; Cejka, J.; Bein, T. *Microporous Mesoporous Mater.* **2003**, *64*, 165.
(187) On, D. T.; Kaliaguine, S. *Angew. Chem., Int. Ed.* **2001**, *40*, 3248.
(188) On, D. T.; Kaliaguine, S. *Angew. Chem., Int. Ed.* **2002**, *41*, 1036.
(189) Waller, P.; Shan, Z.; Marchese, L.; Tartaglione, G.; Zhou, W.; Jansen, J. C.; Maschmeyer, T. *Chem. A Eur. J.* **2004**, *11*, 4970.
(190) Landau, M. V.; Tavor, D.; Regev, O.; Kaliay, M. L.; Herzskowitz, M.; Valtchev, V.; Mintova, S. *Chem. Mater.* **1999**, *11*, 2030.
(191) Landau, M. V.; Vradman, L.; Valtchev, V.; Lezervant, J.; Liubich, E.; Taliankar, M. *Ind. Eng. Chem. Res.* **2003**, *42*, 2773.
(192) Wang, H.; Wang, Z.; Yan, Y. *Chem. Commun.* **2000**, 2333.
(193) Smaihi, M.; Gavalan, E.; Durand, J.-O.; Valtchev, V. P. *J. Mater. Chem.* **2004**, *14*, 1347.
(194) Gautier, B.; Smaihi, M. *New J. Chem.* **2004**, *28*, 457.
(195) Mintova, S.; Mo, S.; Bein, T. *Chem. Mater.* **2001**, *13*, 901.
(196) Mintova, S.; Bein, T. *Microporous Mesoporous Mater.* **2001**, *50*, 159.
(197) Wang, Z.; Larsson, M. L.; Grahn, M.; Holmgren, A.; Hedlund, J. *Chem. Commun.* **2004**, 2888.
(198) Kornic, S.; Baker, M. *Chem. Commun.* **2002**, 1700.
(199) Zhang, Y.; Chen, F.; Shan, W.; Zhuang, J.; Dong, A.; Cai, W.; Tang, Y. *Microporous Mesoporous Mater.* **2003**, *65*, 277.
(200) Walcarius, A.; Ganesan, V.; Larlus, O.; Valtchev, V. *Electroanalysis* **2004**, *16*, 1550.
(201) Castagnola, N. B.; Dutta, P. K. *J. Phys. Chem. B* **1998**, *102*, 1696.
(202) Mintova, S.; De Waele, V.; Schmidhammer, U.; Riedle, E.; Bein, T. *Angew. Chem., Int. Ed.* **2003**, *42*, 1611.
(203) Mintova, S.; De Waele, V.; Hölzl, M.; Schmidhammer, U.; Mihailova, B.; Riedle, E.; Bein, T. *J. Phys. Chem. A* **2004**, *108*, 10640.
(204) Megelski, S.; Calzaferri, G. *Adv. Funct. Mater.* **2001**, *11*, 277.
(205) Calzaferri, G.; Brühwiler, D.; Megelski, S.; Pfenninger, M.; Pauchard, M.; Hennessy, B.; Maas, H.; Devaux, A.; Graf, U. *Solid State Sci.* **2000**, *2*, 421.
(206) Wang, Z.; Wang, H.; Mitra, A.; Huang, L.; Yan, Y. *Adv. Mater.* **2001**, *13*, 746.
(207) Wang, Z.; Mitra, A.; Wang, H.; Huang, L.; Yan, Y. *Adv. Mater.* **2001**, *13*, 1463.
(208) Li, S.; Li, Z.; Yan, Y. *Adv. Mater.* **2003**, *15*, 1528.
(209) Li, Z.; Li, S.; Luo, H.; Yan, Y. *Adv. Funct. Mater.* **2004**, *14*, 1019.
(210) Mintova, S.; Bein, T. *Adv. Mater.* **2001**, *13*, 1880.
(211) Larlus, O.; Mintova, S.; Valtchev, V.; Jean, B.; Metzger, T. H.; Bein, T. *Appl. Surf. Sci.* **2004**, *226*, 155.
(212) Mitra, A.; Cao, T.; Wang, H.; Wang, Z.; Huang, L.; Li, S.; Li, Z.; Yan, Y. *Ind. Eng. Chem. Res.* **2004**, *43*, 2946.
(213) Platas-Iglesias, C.; Elst, L. V.; Zhou, W.; Muller, R. N.; Geraldes, C. F. G. C.; Maschmeyer, T.; Peters, J. A. *Chem. Eur. J.* **2002**, *8*, 5121.
(214) Bresinska, I.; Balkus, K. J., Jr. *J. Phys. Chem.* **1994**, *98*, 12989.
(215) Bouizi, Y.; Valtchev, V.; Bats, N.; Laroche, C.; Rouleau, L. *Adv. Mater.* **2005**, submitted.
(216) Schwartz, A. B. Patent No. US2781225, 1973.
(217) Camblor, M.; Corma, A.; Valencia, S. *Chem. Commun.* **1996**, 2365.
(218) Corma, A.; Navarro, M. T.; Rey, F.; Rius, J.; Valencia, S. *Angew. Chem., Int. Ed.* **2001**, *40*, 2277.
(219) Blasco, T.; Corma, A.; Diaz-Cabanas, M. J.; Rey, F.; Rius, J.; Sastre, G.; Vidal-Moya, J. A. *J. Am. Chem. Soc.* **2004**, *126*, 13414.
(220) Harbuzaru, B.; Paillaud, J.-L.; Patarin, J.; Bats, N. *Science* **2004**, *304*, 990.
(221) Corma, A.; Rey, F.; Rius, J.; Sabater, M. J.; Valencia, S. *Nature* **2004**, *431*, 287.
(222) Bouizi, Y.; Valtchev, V.; Rouleau, L.; Bats, N.; Simon, L. Fr. Pat. Appl. 0400841, 2004.

CM047908Z